PLOS ONE

RESEARCH ARTICLE

Paleoceanography of the Late Cretaceous northwestern Tethys Ocean: Seasonal upwelling or steady thermocline?

Eric Otto Walliser ORCID ⊕ *, Bernd R. Schöne ⊕

Institute of Geosciences, University of Mainz, Mainz, Germany

⊕ These authors contributed equally to this work.
* walliser@uni-mainz.de

Abstract

In this study we attempted to assess whether seasonal upwelling or a steady thermocline persisted at the western margin of the Tethys Ocean during the late Turonian–early Coniacian interval. For this scope, we employed novel and published stable oxygen isotope ($\delta^{18}O$) data of various organisms (bivalves, bivalves, brachiopods, fish and belemnites). New seasonally resolved temperature estimates were based on the $\delta^{18}O$ record of sequentially sampled inoceramid (*Inoceramus* sp.) and rudist (*Hippurites resectus*) shells from the Scaglia Rossa and Gosau deposits of northern Italy and western Austria, respectively. Diagenetic screening was performed using reflected light, cathodoluminescence (CL), scanning electron microscopy (SEM) and stable isotope analysis. Originally preserved $\delta^{13}C$ and $\delta^{18}O$ values were used to characterize the lifestyle of the bivalves and detect vital effects that could have biased oxygen isotope-based temperature reconstructions. Inoceramid $\delta^{18}O$ values provide–for the first time–information on temperatures of Tethyan benthic waters, which were, on average, 14.4 ± 0.6 ˚C and fluctuated seasonally within a range of less than 2 ˚C. Such a thermal regime is in line with the temperatures postulated for late Turonian boreal water masses and support the existence of a cold water supply from the North Atlantic to the Tethyan bottom. Bottom cooling, however, did not affect the shallow water environment. In fact, the rudist-based temperature estimates for shallow water environment revealed a mean annual range of 11 ˚C, between 24 and 35 ˚C (assuming a seasonally constant $\delta18O_w$ = 1.0 ‰), which are among the warmest temperatures recorded over the entire Late Cretaceous. Our findings, thus, suggest a strong thermal and food web decoupling between the two environments. The absence of a seasonal vertical homogenization of different water bodies suggests the existence of a steady thermocline and, therefore, contrasts with the presence of an active coastal upwelling in the region as hypothesized by previous authors.

Introduction

Following the Aptian-early Turonian 'supergreenhouse' event (90–95 Ma) [1,2], the Late Cretaceous world experienced a time interval of significant global cooling [3–5]. Declining

atmospheric pCO$_2$ levels [6] and plate tectonics [4] triggered profound paleoceanographic changes in the North Atlantic sector [4,7]. Numerical climate simulations indicate that deep water production in the North Atlantic was possible during most of the Late Cretaceous [8–10], and geochemical proxy data suggest that migration of cold, high latitude water masses into the equatorial Atlantic Ocean and Central Europe occurred as early as the middle and late Turonian [11–13]. During this interval, North Atlantic waters also flooded the northwestern Tethys Basin [14] increasing the dissolved oxygen levels at the bottom of the ocean [15–17], which drove to the formation of the reddish-pinkish shale, marls and limestones of the Scaglia Rossa Formation [18–20]. A coeval increase of the δ^{18}O values of western Tethyan fish teeth was interpreted as the North Atlantic cooling also affecting the upper ocean waters of the northwestern Tethys [21]. In addition, the existence of an active upwelling system in the region was hypothesized [14]. However, the δ^{18}O values of coeval rudist shells from Austria suggest water temperatures of up to 35 ˚C in shallow water environments, i.e., among the warmest temperatures recorded during the entire Late Cretaceous [22]. Therefore, it is possible that oceanic cooling did not pervade the shallowest habitats at the northwestern margin of the Tethys and thermal decoupling (instead of upwelling) existed between the bottom and the shallow water environments during the late Turonian–early Coniacian.

A fundamental physical parameter employed by modern oceanographers to test such a hypothesis would be the vertical profiling of the temperatures during different seasons [23–25]. Coastal upwelling is mainly governed by wind stress curls and, therefore, it possesses strong seasonal character [26,27]. Hence, the vertical migration of cold bottom waters to the surface usually results in a certain degree of thermal homogenization in the water column for at least part of the year [25]. For ancient water bodies, such seasonally resolved information can be inferred from the geochemical proxy record of fossil bivalves, which coexisted (in geological terms) at different water depths. Late Cretaceous shallow water habitats were dominated by rudist bivalves, which majorly contributed to the formation of peri-Tethyan deposits [28]. Rudist shells, especially those of the elevator morphotypes [29], have been extensively used in sclerochronological studies [22,30–33]. To estimate deeper sub-annual water temperatures, inoceramid shells represent a promising proxy archive. This bivalve taxon colonized nearly all benthic Late Cretaceous marine habitats and were widely distributed in the bottom environments of the Tethys [34].

Rudists and, to a lesser extent, inoceramids have been in the focus of many paleoclimate studies. However, because these taxa lack modern representatives, the validity of their stable isotope values for paleotemperature reconstructions has been questioned in the past [32], in particular for the inoceramids [35–43]. Rudist shells often display a positive correlation between δ^{13}C and δ^{18}O values. In a previous study, this correlation was interpreted as a sign for kinetic isotope effects, which prompted the authors to assume disequilibrium fractionation for the rudist species *Torreites sanchezii* [32]. More recent structure morphological and sclerochronological evidences, however, strongly indicate that such stable isotopic patterns derived from a photosynthetic lifestyle [33,44]. It is known that symbiotic algal activity can strongly affect the δ^{13}C signal of shell [45]. However, photosynthesis does not affect the equilibrium incorporation of oxygen isotopes [45], and photosymbiotic bivalves (e.g., tridacnids) are considered among the most faithful recorders of tropical surface water temperatures (SST) [46–48]. A photosynthetic lifestyle has also been proposed for inoceramids, because some species show morphological traits comparable to modern photosynthetic bivalves [49] and might have lived pseudo-planktonic anchored to floating objects [50]. Yet, the broad environmental tolerance and preferential occurrence of this taxon in rather deep habitats make this assumption not applicable to all inoceramid species [51]. Equilibrium fractionation of oxygen isotopes between shell and water has been demonstrated for several inoceramid taxa [52–55]. However,

previous studies have also hypothesized disequilibrium fractionation related to species-specific vital effects [36,43]. This is because inoceramids often display higher $\delta^{13}C$ values and (sometimes) lower $\delta^{18}O$ values than those of coeval organisms [35–43]. Such isotopic signatures are observed in those inoceramids that colonized dysoxic and H_2S-rich environments (stagnant bottom waters or cold seeps) [43,52,54,56,57], and mimic the $\delta^{13}C$ and $\delta^{18}O$ signals of modern thioautotrophic bivalves [58–61]. In the light of the above, an assessment of the metabolisms of the studied rudist and inoceramid bivalve is required to exclude possible vital effects on the $\delta^{18}O$ records, which can, ultimately, bias the estimation of the paleowater temperatures.

In the present study, we sclerochronologically sampled $\delta^{13}C$ and $\delta^{18}O$ values of well-preserved rudist and inoceramid shells to estimate the sub-annual temperature variability that prevailed in the shallow and deeper water environments of the northwestern Tethyan Ocean during the Late Turonian-Early Coniacian interval (Fig 1). Shallow water seasonal variability was reconstructed by combining novel and published sclerochronological stable isotope data of rudist material from shallow water deposits of the Gosau Formation of Austria. We also present the first temperature reconstruction of the seafloor water temperature that prevailed in the hemipelagic environment of the Tethys. Seasonal temperatures were estimated from sequentially sampled $\delta^{18}O$ values of *Inoceramus* sp. shells from the 'lastame' deposits of the Scaglia Rossa Formation of northern Italy. Prior to using the shells for environmental reconstructions, we performed a detailed diagenetic screening of the shell material by employing a combination of cathodoluminescence (CL), scanning electron microscopy (SEM) and stable isotope analysis of different carbonate phases. Well-preserved $\delta^{13}C$ and $\delta^{18}O$ values were used to discuss the autoecology of the bivalves and the impact of possible vital effects on the paleowater temperature estimates. Additionally, we combined our results with previously published temperature reconstructions of coeval seawaters of the Central European basins to gain information on the vertical temperature gradient of the studied water body. Finally, temperature estimates were used to test the hypothesis of a thermal decoupling between hemipelagic and shallow water environments in study region. The present study highlights the potential of bivalve sclerochronology for palaeoceanographic studies.

Geological settings, material and methods

In the present study we sclerochronologically analyzed the shells of two *Inoceramus* sp. (ID: SNSB-BSPG 1973 VII ?60 A, B) and one *Hippurites resectus* (ID: SNSBBSPG1991X) specimens (Fig 2) stored at the Bavarian State Collection for Paleontology and Geology of Munich. Permission for all analysis performed in this study was granted by the curator of the collection and specimens were permanently stored (under the above mentioned ID-numbers) and made publicly accessible at the Bavarian State Collection for Paleontology and Geology of Munich (Richard-Wagner-Str. 10, 80333 Munich, Germany). The rudist shell was 15 cm long and exhibited distinct growth lines in its outer shell layer (OSL) (Fig 2A). The shell originates from the mixed siliciclastic-carbonate deposits of the 'Atzl Reef' (Gosau Group) exposed near the town of Brandenberg (North Calcareous Alps, Austria). According to paleontological and petrological studies, the limestones of the 'Atzl Reef' were deposited in a shallow subtidal environment [63,64], and previous $\delta^{18}O$-based temperature reconstructions suggest very warm conditions compatible with a Late Cretaceous shallow water habitat [22]. To estimate the full seasonal temperature amplitude that prevailed in this environment, the stable isotope data of our specimen were combined with those of previously published *Vaccinites inaequicostatus* shells [22,65] from the 'Atzl reef' and the strata exposed near the town of Theresienstein (Salzburg, Austria).
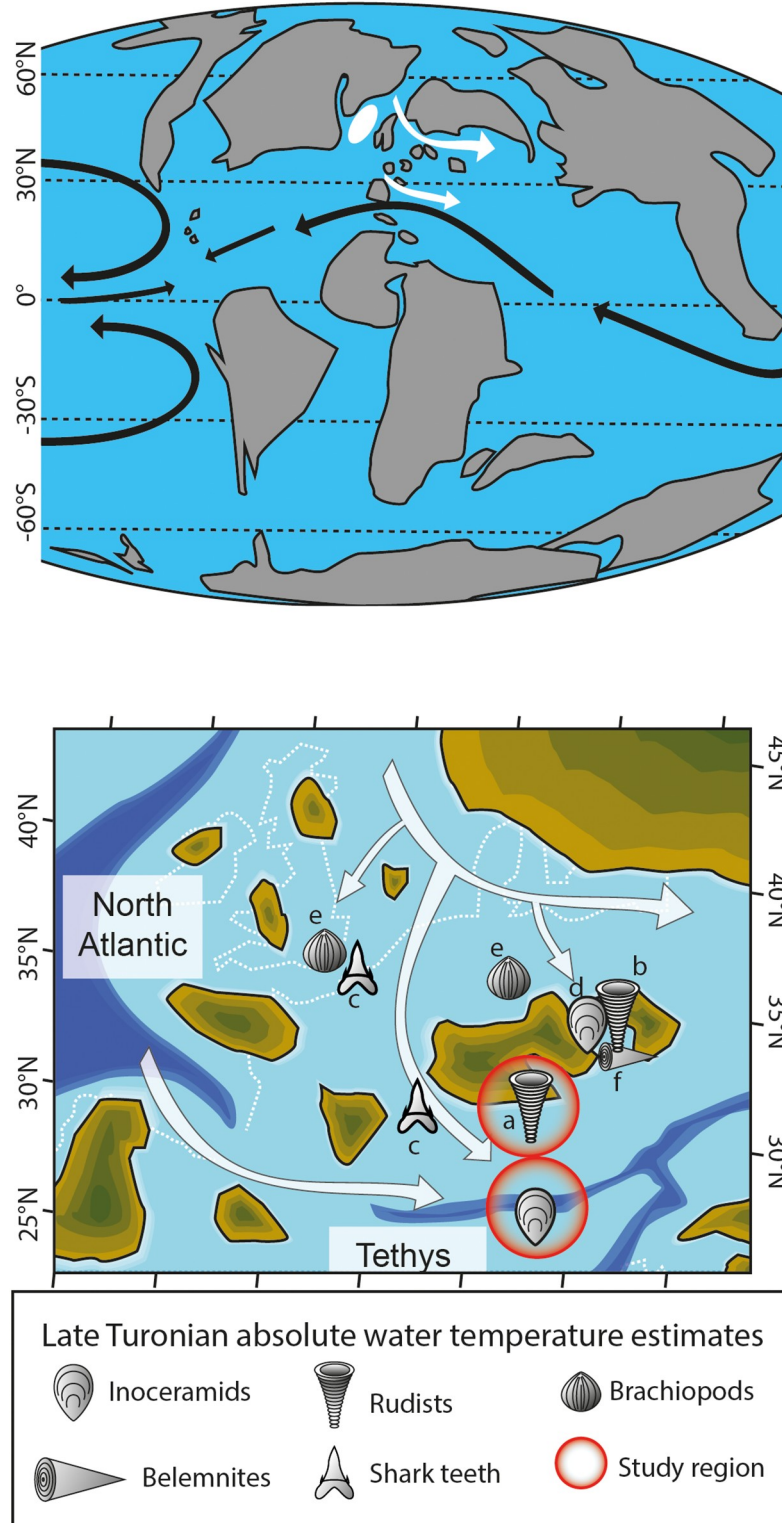
Fig 1. Simplified paleogeography of Earth and the northwestern margin of the Tethys during the late Turonian-early Coniacian interval. (A) Global paleogeography during the Late Turonian (modified from [62]) showing the patterns of the main surface oceanic currents (black arrows). The location of the deep water formation site in the North Atlantic (white circle) [14] and inferred ingression paths of high latitude cold waters onto the Central European shelves and the northwestern Tethys (white arrows) are shown. (B) Paleogeography of the northwestern Tethys

showing possible paths of boreal and North Atlantic water ingression in the study region. The location of the 'Atzl Reef' and the Trento Plateau (i.e., the studied environments) are indicated by the red circles. Symbols show the location of published water temperature estimates in the region derived from the stable oxygen isotope values of (a-b) rudist shells and shark teeth as well as from (d) inoceramid, (e) brachiopod and (f) belemnite remains (cf. Table 2).

https://doi.org/10.1371/journal.pone.0238040.g001

The inoceramid specimens consisted of two internal molds partially covered by fragments of the original OSL (Fig 2E). The specimens were collected from the deposits of the Scaglia Rossa Formation near the town of Sant´Anna d´Alfaedo (Lessini Mountains, northern Italy). The pinkish nodular limestone surrounding the inoceramid allows to constrain the stratigraphic position to the 'lastame' lithozone [66–70]. The studied succession was deposited from the late Turonian to the Coniacian on the Trento Plateau, a hemipelagic rise located at the northern margin of the Tethys few hundreds of km south of the 'Atzl Reef' [66]. Existing estimates of the paleobathymetric range have yielded contrasting results. The occurrence of globotruncanids and the absence of benthic foraminifera in the sediment have been interpreted as suggesting bathyal depths well below the neritic zone [71]. Some authors postulated that the Trento Plateau was situated above the local oxygen minimum zone and suggested water depths between 400 and 700 m [72]. In a more recent study, the presence of radiolitid rudists in the 'lastame' deposits has been interpreted as indicative for water depths near the lower photic zone (ca. 100–150 m) [67].

The studied Gosau deposits belong to the late Turonian ammonite *Subprionocyclus neptuni* and *Prionocyclus germani* zones [73] and strontium isotope values of well-preserved rudist shells from the two localities revealed an upper Turonian-lowermost Coniacian age for the 'Atzl Reef' and an uppermost Turonian-lower Coniacian age for the Theresienstein material [74]. The 'lastame' deposits span from the upper *Marginotrucana scneegansi* to the lower *Dicarinella concavata* planktonic foraminifera zones and are comprised in the nannofossil zone CC12 or UC8[69], which are temporally equivalent to the *S. neptuni* zone [75]. Accordingly, the studied time interval can be constrained to about 2 Ma, between 89 and 91 Ma [75].

Shell preparation, sampling and stable isotope analysis

Fragments were first coated with WIKO metal epoxy resin to avoid breakage during cross-sectioning. Then, a 1 cm-thick slab was cut from the specimen along the direction of growth (Fig 2A, 2B, 2E and 2F). The slabs were finally ground with SiC powders (F300, F800, F1200 grit) on glass plates and polished with a 1 μm Al_2O_3 powder on a Buehler G-cloth.

The state of preservation of the material was evaluated visually, by means of reflected light microscopy as well as using cathodoluminescence (CL) and scanning electron microscopy (SEM). CL microscopy is a non-invasive technique, which uses a high-energy electron beam to identify the distribution of trace elements in minerals [76,77]. For example, low-Mg calcite (LMC) shells with high concentrations of Mn emit a bright orange to reddish CL and are typically regarded as diagenetically altered [53]. SEM analysis was performed on hand-broken fragments of the OSLs to evaluate the preservation of the shell ultrastructures and possible signs μm-scale recrystallization and precipitation of neomorphic material [36,78]. Finally, the stable isotope values of different biotic and abiotic carbonate phases were used to evaluate the effect of diagenesis on the original $\delta^{13}C$ and $\delta^{18}O$ record of the studied bivalve shells.

Carbonate powders (50–120 μm) for $\delta^{13}C$ and $\delta^{18}O$ measurements were collected from the biogenic LMC, from the micrite, and from sparite encrusting the shells and infilling voids (S1 Fig) using a Rexim Minimo dental drill equipped with a 300 μm-diameter conical SiC bit (Gebr. Brasseler GmbH & Co. KG, model number H52 104 003) mounted on a stereomicroscope. To ensure an adequate temporal resolution for seasonal environmental reconstructions,
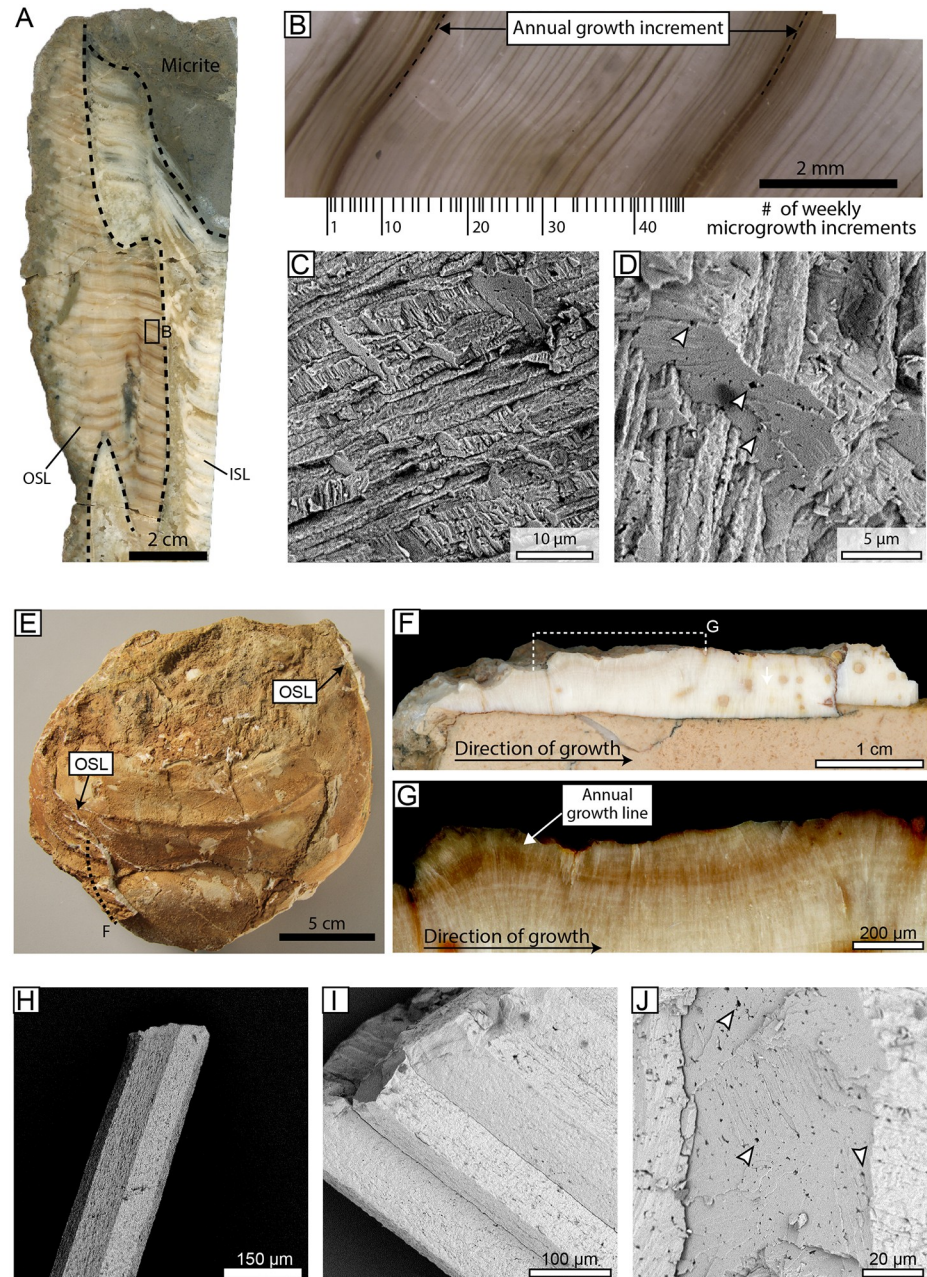
Fig 2. The studied shell material. (A) Cross-section trough the *Hippurites resctus* shell from the 'Atzl Reef' deposits of Brandenberg (Austria) showing marked annual growth lines in the outer shell layer (OSL). (B) At higher magnification, microgrowth increments were easily recognizable. Their number within one annual growth increment (ca. 49) suggests weekly shell growth cycles for the studied *H. resectus* individual. (C) SEM imaging revealed the preservation of the original fibrous prismatic ultrastructure of the OSL and the presence of intra-prismatic voids inside the biomineral units. (E) One of the studied *Inoceramus* sp. fossils from the 'lastame' deposits of Sant´Anna d´Alfaedo (Italy). The inoceramid steinkern is partially covered by original OSL. The dotted line indicates the location of the shell cross-cut depicted in (F). In cross-cut very faint annual growth lines were recognized (F), however, these became more visible after increasing the contrast of the images (G). Under the SEM, the low-Mg calcite prisms of the studied inoceramids displayed smooth surfaces and sharp edges (H) and the absence of neomorphic precipitates between adjacent prisms. (J) The inoceramid prisms also displayed intra-prismatic voids, which were originally filled with organic matrix. ISL = inner shell layer.

https://doi.org/10.1371/journal.pone.0238040.g002

the inoceramid LMC was sampled from the outer to inner surface of the fragment [54], whereas the rudist OSL was sampled following the direction of growth.

Stable carbon and oxygen isotope measurements were performed at the Institute of Geoscience of the University of Mainz. Carbonate powder were digested with a water-free phosphoric acid in He-flushed exetainers at 72 ˚C. The liberated CO_2 gas was then measured in continuous flow mode with a Thermo Finnegan MAT 253 gas source isotope ratio mass spectrometer coupled to a Gas Bench II. Data calibration was performed against a NBS-19 calibrated Carrara Marble distributed by IVA Analysensysteme GmbH ($\delta^{13}C$ = +2.01 ‰; $\delta^{18}O$ = -1.91 ‰). Stable isotope values are given in the δ-notation in parts per mil (‰). The 1σ accuracy (based on long-term analysis) and average 1σ internal precision (based on 8 injections per analyzed sample) for $\delta^{13}C$ values were better than 0.04 and 0.02 ‰, respectively, and better than 0.05 ‰ and 0.03%, respectively, for $\delta^{18}O$ values.

Estimation of water temperatures and $\delta^{18}O$ signal

Since bivalve shells are formed near isotopic equilibrium with the ambient water, their $\delta^{18}O$ values can be used to reconstruct paleowater temperatures [79]. The OSL of rudists and inoceramids was composed of fibrous and prismatic LMC, respectively. Both taxa also produced an aragonitic inner shell layer, which was not preserved in studied specimens. Therefore, in the present study, we employed a paleothermometry equation [80], which is typically used for rudist and inoceramid LMC [22, 45]:

$$T_{\delta 18O}(^{\circ}C) = 16.0 - 4.14 \times (\delta^{18}O_{shell} - \delta^{18}O_w) + 0.13 \times (\delta^{18}O_{shell} - \delta^{18}O_w)^2 \tag{1}$$

whereby, the $\delta^{18}O_{shell}$ and $\delta^{18}O_w$ values are given relative to the VPDB and VSMOW scale, respectively. According to Eq (1), the computation of $\delta^{18}O$-based paleotemperatures requires the knowledge of the water $\delta^{18}O$ signature ($\delta^{18}O_w$). In the present study, we performed temperature calculations considering different $\delta^{18}O_w$ scenarios. For the Late Cretaceous ice-free world, an average oceanic $\delta^{18}O_w$ signal of -1.0 ‰ is typically assumed [81], whereas, climate model simulations suggest an average value of +0.5 ‰ for the Cretaceous Tethyan surface waters [82]. Furthermore, we constructed a model to assess the possible effects of the $\delta^{18}O_w$ changes in the water column on the reconstruction of the vertical temperature gradient. We simulated four scenarios by fitting polynomial functions to observational $\delta^{18}O_w$ data from the first 900 m water depths of tropical Indian, Pacific and Atlantic Ocean as well as the Gulf of Mexico [83]. Additionally, we employed the Late Cretaceous vertical $\delta^{18}O_w$ gradient simulated using the GENESIS-MOM numerical climate model [82]. The modeled gradients were used to calculate the vertical temperature amplitude (ΔT) required to justify the shell $\delta^{18}O_{shell}$ difference between the surface (10 m) and bottom environments (900 m water depth).

Results

Rudist material

The OSL of the *Hippurites resectus* specimen exhibited marked dark brown major growth lines, which divided the shell growth pattern into 4–5 mm broad growth increments (Fig 2A). In turn, major growth increments were subdivided by thin microgrowth lines into 40–50 microgrowth increments of 20–100 μm width (Fig 2B). Under the CL, the OSL was non-luminescent, and SEM imaging revealed the preservation of the original fibrous calcitic ultrastructure of the shell. Occasionally, μm-scale neomorphic precipitates were observed on individual calcitic fibers. The presence of intra-crystalline voids, however, suggest that recrystallization remained only very superficial (Fig 2C and 2D). Orange to bright red luminescence was

Table 1. Stable oxygen and carbon isotope values of the different carbonate phases analyzed in this study.

| Bivalve taxon (specimen ID) | Carbonate phase | $\delta^{13}C_{shell}$ | | | $\delta^{18}O_{shell}$ | | | |
		Min (‰)	Average ± 1 σ (‰)	Max (‰)	Min (‰)	Average ± 1 σ (‰)	Max (‰)	# of isotope samples
Inoceramus sp. SNSB-BSPG 1973 VII ? 60	Sediment	2.44	2.60 ± 0.12	2.83	-1.50	-1.32 ± 0.23	-0.86	6
	Sparitic calcite	2.17	2.35 ± 0.15	2.55	-2.07	-1.80 ± 0.19	-1.55	5
	Shell A							
	OSL Fragment 1	2.86	3.07 ± 0.13	3.38	-0.65	-0.52 ± 0.05	-0.42	35
	OSL Fragment 2	2.24	2.73 ± 0.19	3.00	-1.44	0.71 ± 0.22	-0.45	24
	Shell B	2.05	2.54 ± 0.24	2.95	-1.00	-0.74 ± 0.17	-0.51	21
Hippurites resectus (SNSBBSPG1991X)	Sediment	-	0.46	-	-	-3.18	-	1
	Sparitic calcite	-0.39	-0.88	1.39	-9.40	-7.16	-4.92	2
	OSL	1.08	1.67 ± 0.28	2.12	-4.02	-3.18 ± 0.28	-2.85	73

emitted by the sparitic cements, which replaced the original aragonitic shell layer of the rudist and exhibited the most negative $\delta^{18}O$ values (-9.38 ‰) (Table 1). The $\delta^{18}O$ value of the micrite (-3.18 ‰) fell within the range of stable isotope oxygen values measured in the OSL (-4.92 to -2.85 ‰). The micrite $\delta^{13}C$ value (0.46 ‰) was slightly lower than those measured in the biogenic LMC ($\delta^{13}C$ = 1.08–2.12 ‰) (Fig 3A; Table 1). Sequentially sampled $\delta^{13}C$ and $\delta^{18}O$ data from the OSL were positively correlated (R = +0.82; R^2 = 0.68; p >0.01) (Fig 3A) and exhibited five consecutive oscillations, with the major growth lines coinciding with the $\delta^{18}O$ and the $\delta^{13}C$ minima (Fig 4A).

Stable isotope values are given for the sediment, the sparitic calcite and the shells of the *Inoceramus* sp. and *Hippurites resectus* specimens.
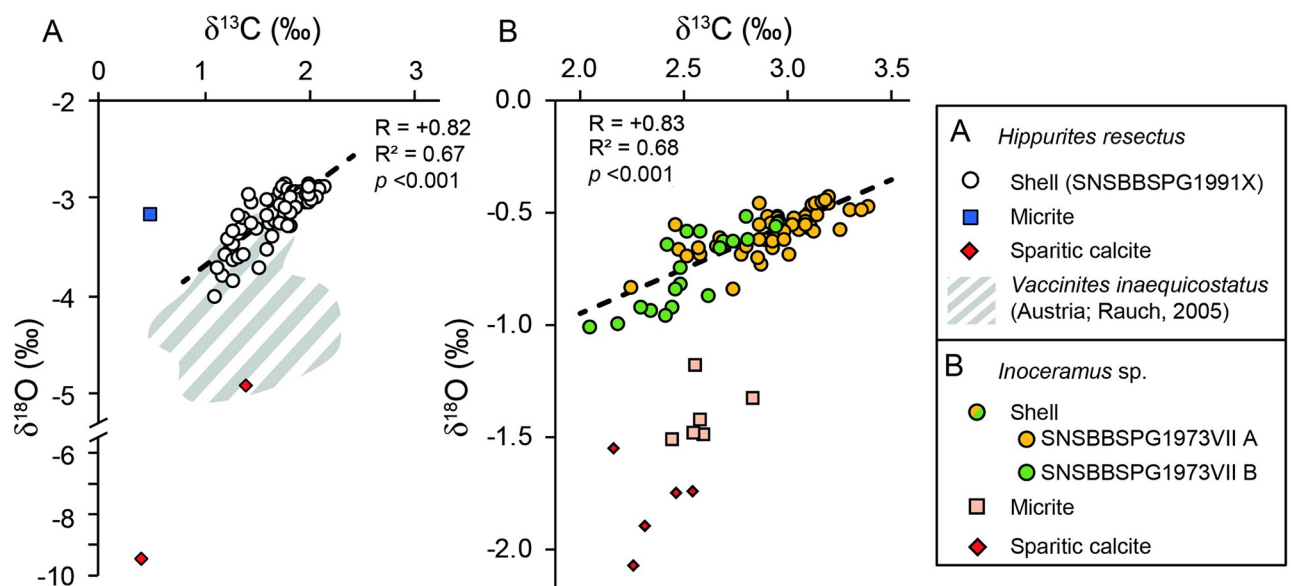

Fig 3. Plots of the $\delta^{13}C$ and $\delta^{18}O$ values of the carbonates analyzed in this study. These include burial sparite, micrite, and the low-Mg calcite shells of the studied inoceramid and rudist material. (A) The stable isotope values of the *Hippurites resectus* shell are positively correlated (R = +0.82; R^2 = 0.67; p-value < 0.001) and plot in the upper range of previously published $\delta^{13}C$ and $\delta^{18}O$ values of coeval the *Vaccinites inaequicostatus* rudists [65] (shaded area). (B) The studied *Inoceramus* sp. specimens also display a positive correlation (R = +0.83; R^2 = 0.68; p-value < 0.001) and does not overlap with the stable isotope values of diagenetic altered phases (micrite and sparite).
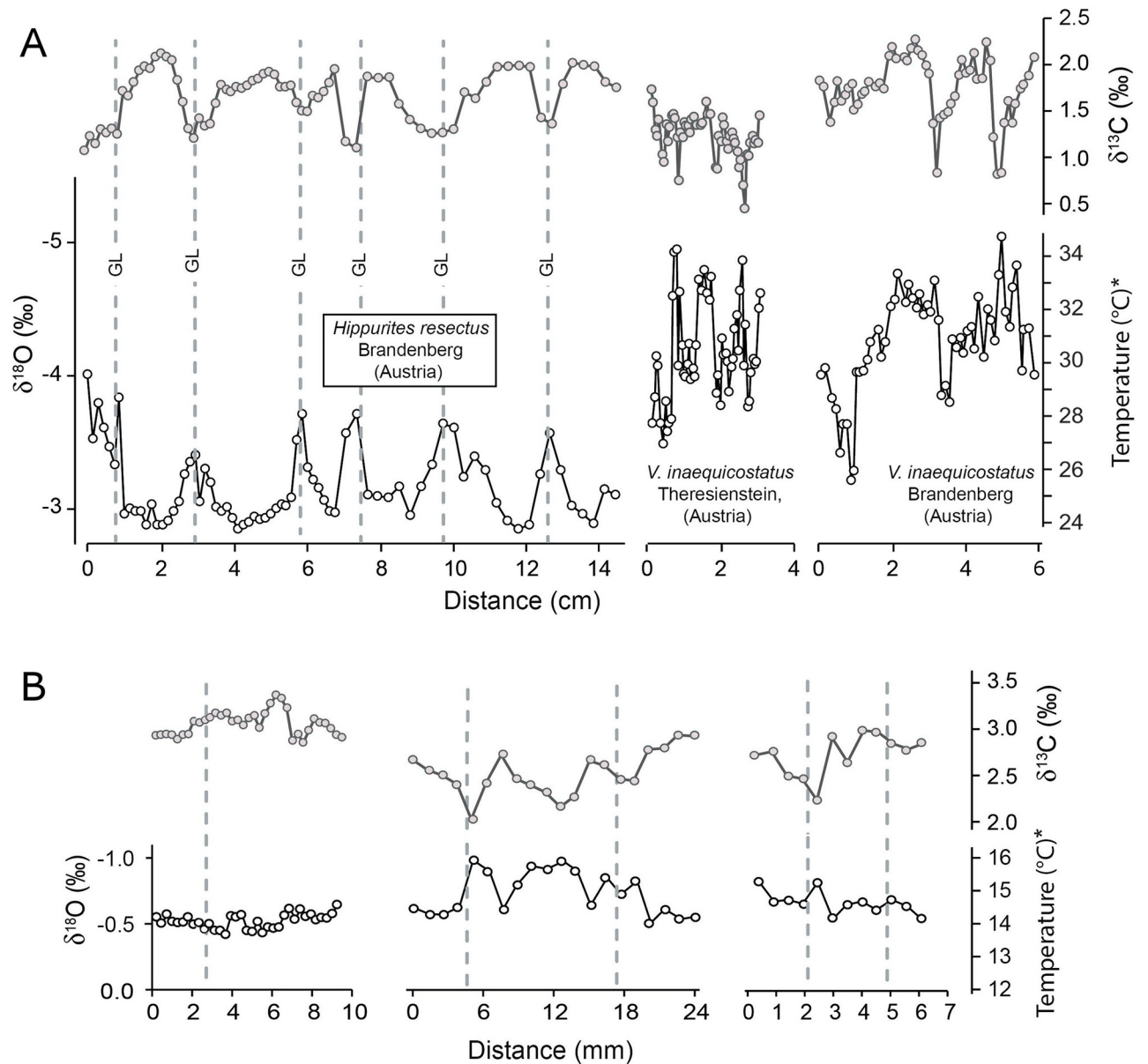
Fig 4. Sequentially sampled δ¹³C and δ¹⁸O values the studied rudist and inoceramid shells and temperatures reconstructed thereof. (A) In the *Hippurites resectus*, the position of the growth lines (GL; gray dotted lines) coincided with the δ¹⁸O minima, which suggest that shell growth occurred mostly during winter. In comparison, the shape of the δ¹⁸O curves of the coeval *Vaccinites inaequicostatus* [65] suggest a predominant summer shell growth. (B) In the *Inoceramus* sp. specimens, growth lines were located shortly before the seasonal δ¹⁸O minima, suggesting that the full seasonal temperature amplitude was recorded by the bivalves. Temperatures were computed assuming an average ocean δ¹⁸O$_{water}$ value of -1.00 ‰ [81].

https://doi.org/10.1371/journal.pone.0238040.g004

Inoceramid material

The inoceramid shells exhibited sharply defined polyhedral prisms, and faint major growth lines were identified when viewed under a reflected-light microscope (Fig 2F and 2G). Under CL, the studied inoceramid shell fragment was non-luminescent to dark blue luminescent, whereas, orange luminescence was emitted by the micrite and the sparite infilling the

Table 2. Temperature estimates used for the reconstruction of the vertical water temperature gradient at the northwestern margin of the Tethys.

Environment (water depth)	Proxy archive (Taxon)	Locality	Age	Reference	$T_{\delta 18O}$		
					Min (˚C)	Average ± 1σ (˚C)	Max (˚C)
Shallow water (2–10 m)	Rudist OSL (*Hippurites resectus*)	‚Atzl Reef‘, Brandenberg (Austria)	Late Turonian/ earliest Coniacian	**This study**	24.1	25.6 ± 1.3	29.7
	Rudist OSL (*Vaccinites Inaequicostatu*)	‚Atzl Reef‘, Brandenberg (Austria)	Late Turonian/ earliest Coniacian	[22,65]	25.9	30.9 ± 1.9	35.0
	Rudist OSL (*Vaccinites Inaequicostatu*)	Theresienstein Strobel (Austria)	Latest Turonian/ early Coniacian	[22,65]	27.2	30.6 ± 1.8	34.4
	Rudist OSL (*Radiolites undulatus*)	Kučlín (Czech Republic)	Turonian	[84]	32.9	33.8	34.7
Upper ocean water (<150 m)	Fish tooth enamel and enameloid (Lamniforme, undetermined)	Somme, Adèrche (France)	Turonian, Coniacian	[21]	21.0	24.0	28.4
Central European shelf (50-150m)	Inoceramid OSL (*Inoceramus hercules*)	Úpohlavy warking quarry (Czech Republic)	Late Turonian	[55]	16.2	19.7 ± 1.0	24.9
	Brachiopod shell* (rhynchonellids, terebratulids)	Dover, Kensworth, Lewes (southern England); Söhlde, Hoppenstedt (northern Germany).	Late Turonian	[12]	16.0	18.6 ± 1.1	22.0
	Belemnite rostrum (*Praeactinocamax bohemicus*)	Úpohlavy warking quarry (Czech Republic)	Late Turonian	[85]	16.4	14.8	15.2
Hemipelagic water (Trento Plateau) (150–200 m)	Inoceramid OSL (*Inoceramus* sp.)	Sant´Anna d´Alfaedo (Italy)	Late Tur./ Con.	**This study**	13.6	14.4 ± 0.6	16.0

foraminiferan tests. The latter exhibited the lowest $\delta^{13}C$ (+2.35 ± 0.14 ‰; ± 1σ) and $\delta^{18}O$ values (-1.80 ± 0.17 ‰; ± 1σ), whereas slightly more positive values were measured in the micrite ($\delta^{13}C$ = +2.60 ± 0.11 ‰; $\delta^{18}O$ = -1.32 ± 0.22 ‰; ±1σ) (Fig 3B; Table 1). Under the SEM, LMC prisms were tightly packed, and no neomorphic precipitates were observed within the inter-prismatic space (Fig 2I). The individual biomineral units displayed smooth surfaces and sharp edges, and preserved intra-crystalline voids, visible in cross-sections (Fig 2H and 2J). The inoceramid LMC yielded the most positive $\delta^{13}C$ and $\delta^{18}O$ values, which were, on average, +2.83 ± 0.13 ‰ and -0.61 ± 0.13 ‰ (± 1σ), respectively (Fig 3B; Table 1). Shell $\delta^{13}C$ values fluctuated between +2.04 and +3.38 ‰, whereas the $\delta^{18}O$ data oscillated within a much narrower range, i.e., between -0.99 and -0.42 ‰ (Fig 4B). The $\delta^{13}C$ and $\delta^{18}O$ data were positively correlated (R = +0.83; R^2 = 0.68; p < 0.01) (Fig 3B), and the faint growth lines were located shortly after the local maxima (Fig 4B).

Water temperature estimates

In combination with previously published $\delta^{18}O_{shell}$ values of the rudist *Vaccinites inaequicostatus* from the same locality and slightly younger Gosau deposits [22,65], our *H. resectus* data suggest an environmental $\delta^{18}O$ amplitude of 2.28 ‰ (-5.10 to 2.85 ‰). Assuming a seasonally constant $\delta^{18}O_w$ of -1.00 ‰, these $\delta^{18}O$ values translate into SST between 24 and 35˚C (Fig 4A; Table 2). Temperature estimates become 7–8 ˚C higher (31 to 43 ˚C) if a $\delta^{18}O_w$ value of +0.5 ‰ [82] is applied. The $\delta^{18}O$ values of the studied inoceramid shell yielded paleowater temperatures between 13–14 and 16 ˚C (Fig 4B) as well as 21 and 23 ˚C assuming a $\delta^{18}O_w$ value of -1.0 ‰ and +0.5 ‰, respectively. Hence, our temperature estimates suggest an average vertical ΔT value of 14–15 ˚C between the shallow and bottom water environment if a constant vertical $\delta^{18}O_w$ value is assumed. Simulated vertical changes in $\delta^{18}O_w$ signals suggest vertical ΔT gradients between 14 and 19 ˚C, whereby the assumed water depth plays an important role in the

Atlantic and Gulf of Mexico scenario. The Late Cretaceous and Indian Ocean settings yielded the most conservative ΔT outputs (13–14 ˚C), which are close to the ΔT value calculated assuming a constant $\delta^{18}O_w$ value.

Water temperatures were compiled using novel and published skeletal $\delta^{18}O$ data. Temperatures were estimated assuming an average water $\delta^{18}O$ signature of -1.00 ‰ [81]. Brachiopod-derived temperature should be considered with caution, because these organisms may have not fractionated oxygen isotopes in equilibrium with the ambient water.

Discussion

State of preservation

The reconstruction of paleowater temperatures from $\delta^{18}O$ values requires a detailed diagenetic screening of the biogenic carbonates. This is because accidental sampling of diagenetically altered shell portions can lead to an overestimation of the actual paleowater temperature. The OSL of both analyzed bivalve species consisted of LMC, which is a carbonate polymorph considered to be fairly resistant against diagenetic alteration. As suggested by the presence of original macrogrowth and microgrowth lines, the studied shells did not undergo major recrystallization during burial. Likewise, at a microscopic scale we did not observe mineral modification. The SEM analysis of the rudist and the inoceramid OSL revealed well-defined fibrous prismatic (Fig 2C and 2D) and prismatic (Fig 2H–2J) aggregates, respectively. Particularly, the presence of intra-prismatic voids (Fig 2D and 2J), which are supposed to have been originally filled with intra-crystalline organic matter [86,87], suggest that alteration of the biomineral units (if present) remained only very superficial. In previous sclerochronological studies, this feature was considered to be indicative for very good preservation and a discriminant factor for $\delta^{18}O$-based temperature reconstructions [31,32,86,87].

The well-developed $\delta^{13}C$ and $\delta^{18}O$ cycles measured in the *Hippurites resectus* specimen (Fig 4A) allowed us to confidently exclude a resetting of the original geochemical signal during burial [88]. Hence, the stable isotope values were considered to reflect environmental seasonality. The narrow $\delta^{13}C$ (1.0 ‰) and $\delta^{18}O$ (0.40 ‰) fluctuations measured in the inoceramid shells required a more detailed evaluation. In fact, such reduced stable isotope amplitudes can also result from geochemical resetting. The sparite, which exhibited the lowest $\delta^{13}C$ and $\delta^{18}O$ values, is typically formed during burial and directly precipitates from pore fluids [89]. Therefore, its stable isotope values can be considered as the isotopic endmember of the diagenetic alteration. Accordingly, increasingly altered carbonate material should show a progressive trend toward the $\delta^{13}C$ and $\delta^{18}O$ values of the sparite [90]. Such trend was visible in the micrite (Fig 3B), which exhibited $\delta^{13}C$ values (+2.60 ± 0.11 ‰) coherent with the bulk stable carbon isotope data of other late Turonian-Coniacian Scaglia Rossa successions from Central Italy [91]. The relative uniformity between the isotopic signal of the micrite and the sparite suggests a closed diagenetic system, in which the stable isotope composition of the pore fluids was dominated by the dissolution of the host rock [92]. Such a condition greatly increases the preservation potential of the original stable isotope signature of biogenic calcite [92]. This is also suggested by the fact that inoceramid $\delta^{18}O$ and (partially) $\delta^{13}C$ values were more positive than those of the micrite. Accordingly, isotopic exchange between LMC and pore fluid during burial was likely subordinated, and possible minor changes in the original stable isotope signature remained within the analytical uncertainty. Furthermore, the measured stable isotope oscillations were similar to those observed in other Late Cretaceous bivalves (including inoceramids) [43,53,93] living in deeper settings. In the light of the above, the inoceramid $\delta^{13}C$ and $\delta^{18}O$ values were considered to reflect the near-original signature and, therefore, suitable for paleoenvironmental reconstructions.

Stable isotope seasonality in the studied environments

The shallow water environment.   The striking feature of the stable isotope record of the studied *Hippurites resectus* shell is the robust correlation between the δ^{13}C and δ^{18}O values (Fig 3A). It is highly unlikely that this stable isotope pattern resulted from kinetic fractionation effects, because rudists precipitated their shells in isotopic equilibrium with the ambient water [32]. Correlation between δ^{13}C and δ^{18}O has been observed in many rudist species [33,65] and is a typical feature observed in modern photosymbiont-bearing bivalves, e.g., tridacnids [45,46]. In photosymbiotic bivalves, such a trend results from the enhanced uptake of ^{12}C from the ambient water by the symbiotic algae during periods of high insolation and warm water conditions (i.e., more negative shell δ^{18}O values) [45]. Although controversially debated in the past [28], recent studies provided morphological [44] and sclerochronological [32] evidence supporting a photosymbiotic lifestyle for at least some species of elevator rudists. A further hint for a photosymbiotic lifestyle for *H. rectus* is given by the growth increment counting. The number of microgrowth increments between the annual growth lines (~48) is almost two-fold the number of fortnight cycles (~25) expected to have occurred during a Late Cretaceous year [94]. This suggest that the studied *H. resectus* bivalve grew with a weekly periodicity and formed its shell almost year-round. These two features are also usually observed in modern algae-bearing tridacnids [45] and in other supposedly photoautotrophic rudists [33].

The cuspate shape of the δ^{18}O chronology and the occurrence of the growth lines at the seasonal δ^{18}O minima indicates that most of the shell production occurred during the cold part of the year [95]. Shell accretion rates strongly decreased with the onset of the seasonal warming and possibly shortly ceased during the summer extremes. Thus, the measured summer δ^{18}O values are strongly affected by time-averaging and do not allow to properly resolve the information on the seasonal temperature maxima that prevailed in the studied environment. Late Turonian–early Coniacian summer temperature information of the Gosau environment are provided by published δ^{18}O data of sequentially sampled *Vaccinites inaequicostatus* shells [22,65]. In the frame of the present study, it not possible to precisely determine the timing of shell formation of these rudists, because the position of the growth lines was not reported by the authors, and congeneric bivalves show a large inter-specific variability in the timing of annual growth line formation [30,32,95,96]. However, as shown in Fig 4A, the δ^{18}O values of *V. inaequicostatus* follow an opposite trend as observed in the *H. resectus* shell indicating a predominant summer growth season. The reduced overlapping of the δ^{18}O values with those of *H. resectus* can be interpreted as a prolonged shell growth stop during the colder part of the year. However, because of the lower sampling resolution as employed here, the reduced overlapping of the two datasets can also be explained by the larger time averaging of the δ^{18}O values near the annual growth lines. Nevertheless, the data clearly indicate the existence of contrasting shell growth strategies between the two rudists, a phenomenon also known from modern bivalve cohorts [97]. Thus, by combining the δ^{18}O data from the two taxa it is possible to estimate a seasonal isotopic amplitude of 2.25 ‰ and seasonal extremes of -5.10 ‰ and -2.85 ‰, for the studied shallow water setting.

The hemipelagic environment.   The validity of inoceramid stable isotope data for paleoclimate reconstructions has been questioned in the past. This is because some taxa likely harbored symbionts, which affected their stable isotope data [43,52,54]. Because of the low or even absent light intensity excepted at the inferred water depth of the Trento Plateau, a photosynthetic lifestyle for studied *Inoceramus* sp. is unlikely. However, even if present, a photoautotrophic metabolism does not represent an obstacle to the reconstruction of paleowater temperatures, because algal activity does not affect the δ^{18}O values of the bivalve hosts [47,48]. The pervasive presence of authigenic hematite [15–17] in the studied deposits clearly indicate

the existence highly oxygenated waters [18–20]. Therefore, the presence of high levels of H_2S and dysoxic conditions near the sea floor can be confidently excluded. Such conditions, however, were indispensable to sustain a thioautotrophic metabolism. Thus, studied *Inoceramus* sp. shells were likely not subject to chemosymbiotic disequilibrium fractionation effects.

Furthermore, isotopic equilibrium fractionation is also suggested by the good agreement of $\delta^{18}O$ values with those reported in the literature for other carbonate secreting organisms. The $\delta^{18}O$ data of the studied inoceramid shells (-1.44 – -0.42 ‰) fall well into the $\delta^{18}O$ range of late Turonian/early Coniacian North Atlantic benthic foraminifera (-1.5 – -0.6 ‰), for which equilibrium fractionation can confidently be assumed [4]. At the same time, our $\delta^{18}O$ values data were slightly more positive than those measured in coeval mollusk LMC from the shelf deposits of Central Europe. Late Turonian inoceramid and belemnite skeletons from the deposits of the Hitch Wood Event (i.e., the coldest interval of the late Turonian) in the Bohemian Basin (western Czech Republic) exhibit $\delta^{18}O$ values between -2.46 and -1.06 ‰ [55] as well as -0.81 and -0.62 ‰ [49], respectively (Fig 5). The belemnite data were derived from the rostrum of a *Praeactinocamax bohemicus* specimen, a belemnite species that exclusively lived within inner shelf waters of the Bohemian Basin [49]. The stable isotope signature of the *Inoceramus* sp. also compares well with the average $\delta^{18}O$ values of brachiopods (-1.33 ‰) from the Hitch Wood Event deposits of the Anglo-Paris Basin and the Lower Saxony Basin [12]. A similarity between the $\delta^{18}O$ values of these two organisms, however, should be taken with caution, because brachiopod $\delta^{18}O$ values can be affected by non-equilibrium isotopic fractionation [12,98,99]. Our Tethyan inoceramids also display more positive $\delta^{18}O$ values than those of subtropical oysters from younger deposits of the Western Atlantic for which isotopic equilibrium with the ambient water are very likely [100].

The measured seasonal $\delta^{18}O$ fluctuations (< 0.5 ‰) are also compatible with the reduced seasonality expected for marine waters at the postulated depths (lower photic zone or deeper) of the studied environment [67,71,] and compare very well with the stable isotope fluctuations recorded by mollusks from other Late Cretaceous hemipelagic benthic environments. Seasonal $\delta^{18}O$ oscillations of 0.5 ‰ were recovered from Turonian-Coniacian inoceramids from the southern North Atlantic, for which equilibrium isotopic fractionation was inferred [53]. Our $\delta^{18}O$ range also compares very well with the seasonal $\delta^{18}O$ fluctuations reconstructed from deep water arcoid bivalves from the Coniacian [101] and Campanian [43,93]. Proxy-development studies on modern arcoids clearly indicate equilibrium isotopic fractionation for this taxon [97,102]. Hence, in the light of the above, it can be assumed that the studied *Inoceramus* sp. bivalves formed their shells near equilibrium with the oxygen isotope signature of the ambient water, as postulated for other inoceramid species [52–55].

The analysis of the inoceramid growth patterns revealed that faint microgrowth lines were not uniformly distributed across the shell transect, but rather occurred as sporadic bundles. This suggests the absence of major seasonal variations in shell growth rate. Although not common in modern bivalves [103], year-round shell growth has also been suggested for other inoceramid species from Central Europe [55], the Western Interior Seaway of the USA [54] and the North Atlantic Ocean [53]. Furthermore, the observed growth lines were located shortly after the seasonal $\delta^{18}O$ minima indicating that shell accretion rates of the studied *Inoceramus* sp. slowed down during decreasing water temperatures. Hence, the individuals captured in their shells information on both seasonal environmental extremes [95]. In other words, unlike *H. resectus*, the time averaging did not affect the record of the seasonal $\delta^{18}O$ minima and maxima, which allows the estimation of the full annual temperature amplitude for the benthic environment of the Trento Plateau.

The fluctuation of the $\delta^{13}C$ values (1.34 ‰) indicates the presence of sub-annual variations in the incorporation of carbon isotopes. Symbiotic activity is known to have a major impact
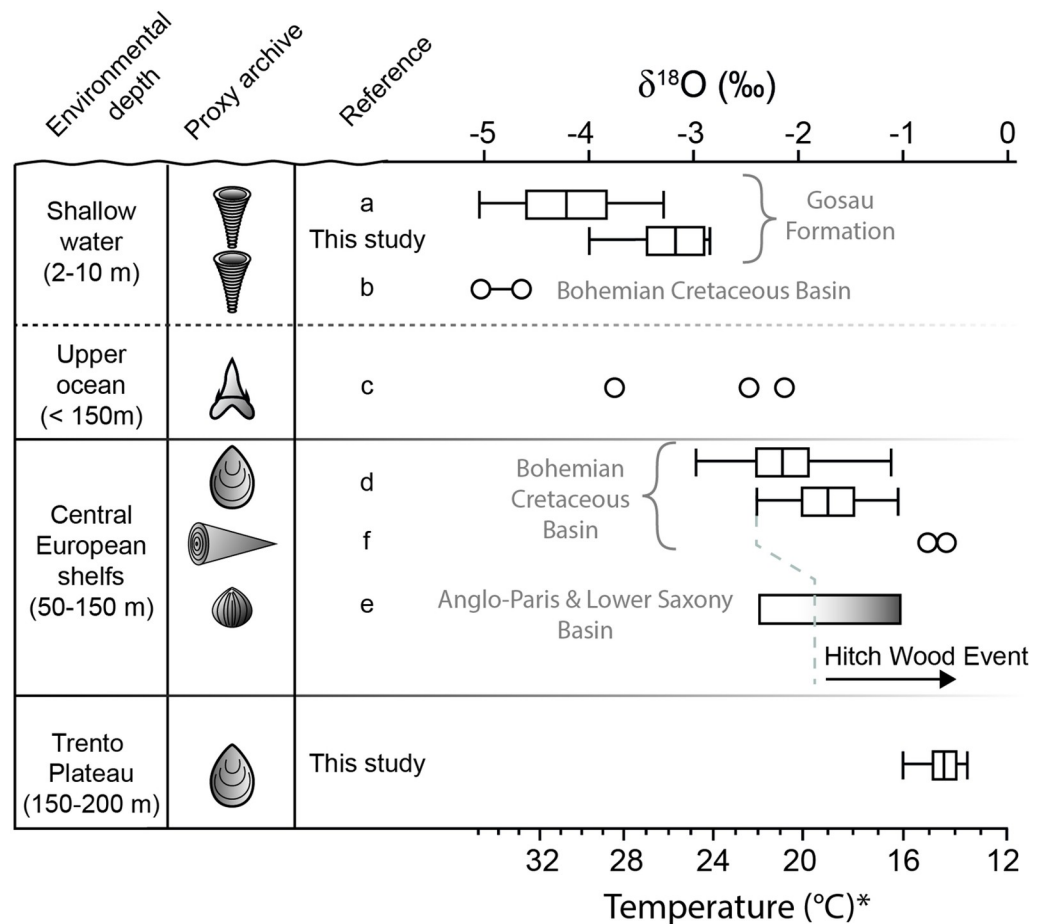
*Assuming seasonally constant $\delta^{18}O_w$ signal of -1.0 ‰

Fig 5. The reconstructed vertical temperature gradient at the northwestern margin of the Tethyan Ocean. Values were compiled from novel and published data. Seasonally resolved temperature estimates are shown as box plots, whereas temperature ranges are shown as bars. Dots represent the temperature estimates based on single $\delta^{18}O$ values. Temperature estimates for the shallow and upper ocean waters derived from stable oxygen isotope data of (a-b) rudist shells [22,65,84] and (c) shark teeth [21]. Temperature information for deeper environments were derived from (d) inoceramid [55] and (e) brachiopod shells [12] as well as from a (f) belemnite rostrum [85]. The Hitch Wood Event represents the coldest interval of the late Turonian. Temperatures were computed assuming an average ocean $\delta^{18}O_{water}$ value of -1.00 ‰ [81].

on the $\delta^{13}C$ of bivalve shells [45]. However, as discussed above, a symbiotic lifestyle for the studied inoceramids can be excluded. In asymbiotic bivalves, changes in $\delta^{13}C$ values of bivalve shells are regarded as reflecting variations in trophic conditions and have been employed to reconstruct past primary production [104–108]. Particularly for inoceramids, $\delta^{13}C$ variations were suggested to indicate changes in food availability in Cretaceous benthic environments [53,54]. This is because the particulate organic matter in seawater has a very negative $\delta^{13}C$ value (< -20‰) [109,110] and contributes up to 10% of the carbon incorporated into the bivalve shells [45]. Additionally, due to organic matter remineralization, increasing concentrations of organic matter in the water column can increase ^{12}C in the dissolved organic carbon (DIC) pool. The DIC, in turn, is the major source (up to 90%) of carbon for bivalve shell production [45]. Therefore, the observed $\delta^{13}C$ fluctuations of the studied inoceramid shell most likely indicate seasonal fluctuations in the availability of food at the seafloor [43,45,54]. For the

benthic environment of the Demerara Rise it was postulated that food supply was provided by primary producers snowing from surface waters [53].

Water temperature estimates

Estimates of water temperature from biogenic $\delta^{18}O$ data strongly depends on the assumption of a plausible $\delta^{18}O_w$ value for the studied environment [79]. For Late Cretaceous marine waters, this assumption can be particularly challenging. Most of the existing $\delta^{18}O$-based paleothermometry studies employed an average $\delta^{18}O_w$ value of -1.0 ‰ [22,30–33,43,53,93] assuming a Late Cretaceous ice-free world [81]. Accordingly, our shallow water $\delta^{18}O$ data suggest a seasonal temperature amplitude of 11.0 ˚C and seasonal extremes of 24 and 35 ˚C (Fig 5). Such reconstructions, however, might underestimate the actual temperatures that prevailed in the studied surface environment. In fact, it should be kept in mind that the $\delta^{18}O_w$ value of -1.0 ‰ is inferred on a global average and does not account for possible spatial heterogeneity in water isotope signatures of the Cretaceous oceans. Late Cretaceous climate simulations suggest an increase of $\delta^{18}O_w$ values towards the equator and a $\delta^{18}O_w$ signature ranging between +0.3 and +0.5 ‰ for the tropical Tethyan surface waters [82]. This $\delta^{18}O_w$ signature compares well with the upper range of $\delta^{18}O_w$ values estimated for open marine sub-tropical Gulf of Mexico (0.41–0.59 ‰) derived from carbonate clumped isotope (Δ_{47}) data of Late Cretaceous mollusk shells [100]. Applying such $\delta^{18}O_w$ values to the paleothermometry Eq (1), the estimated paleotemperatures increase by up to 6 ˚C. The resulting annual mean SST of 37 ˚C agrees with existing SST estimates from $\delta^{18}O_w$-independent proxies. TEX$_{86}$ data from tropical-equatorial paleolatitudes suggest annual average SSTs of ca. 35 ˚C during the late Turonian-Early Coniacian interval [10,111].

Seasonal SST oscillations of 11˚C (assuming an invariant $\delta^{18}O_w$ signature) have been considered to be coherent with the mid-Cretaceous greenhouse interval [22], but are larger than the maximum annual SST range observed at modern tropical latitudes [112] (Fig 6A). However, it can be presumed that late Cretaceous surface waters experienced seasonal changes in the $\delta^{18}O_w$ signature, which should be considered in $\delta^{18}O$-based temperature estimates. Assuming a tropical monsoon climate similar as today, the cumulative effect of enhanced precipitation (lowering of the $\delta^{18}O_w$ signal) and increasing SSTs, and *vice versa* enhanced evaporation (rising $\delta^{18}O_w$ signal) and decreasing SSTs, would result in a dampening of the estimated annual temperature ranges (Fig 6A). For example, assuming a seasonal $\delta^{18}O_w$ fluctuation of 1.5 ‰, as observed in some modern tropical seas [83], our carbonate $\delta^{18}O$ data would yield into an annual SST amplitude of 3.5 ˚C (Fig 6A).

Assuming a $\delta^{18}O_w$ signature of -1.0 ‰, the inoceramid $\delta^{18}O$ data translate into temperatures ranging between 13–14 and 16 ˚C for benthic waters on the Trento Plateau, which fall in the lower range of temperatures estimated for the Central European shelves during the Hitch Wood Event (14–21˚C) [12,55,85]. Climate simulations, however, indicate that $\delta^{18}O_w$ could have increased by up to 0.4 ‰ in the first hundreds of meters below sea surface [82]. Assuming a similar trend for the Tethys ocean, $\delta^{18}O_w$ values in the upper water body of the study region might have been as high as 0.9 ‰, shifting our $\delta^{18}O$-based estimates to 22–26 ˚C. Bivalve Δ_{47} data from younger Late Cretaceous deposits of North America suggest similar temperatures (22–23 ˚C) for open marine waters of the Gulf of Mexico. Therefore, it is possible that Tethyan deep waters $\delta^{18}O_w$ were more positive than previously assumed. On a seasonal scale, temperature oscillations of < 2 ˚C are in line with data from other Late Cretaceous hemipelagic environments [43,53,93,101]. Furthermore, our ΔT estimates fall within the annual temperature amplitude observed in modern tropical oceans between 150 and 400 m water depth (Fig 6B), where sub-annual variations in $\delta^{18}O_w$ are very constrained [83]. Therefore, it can be assumed
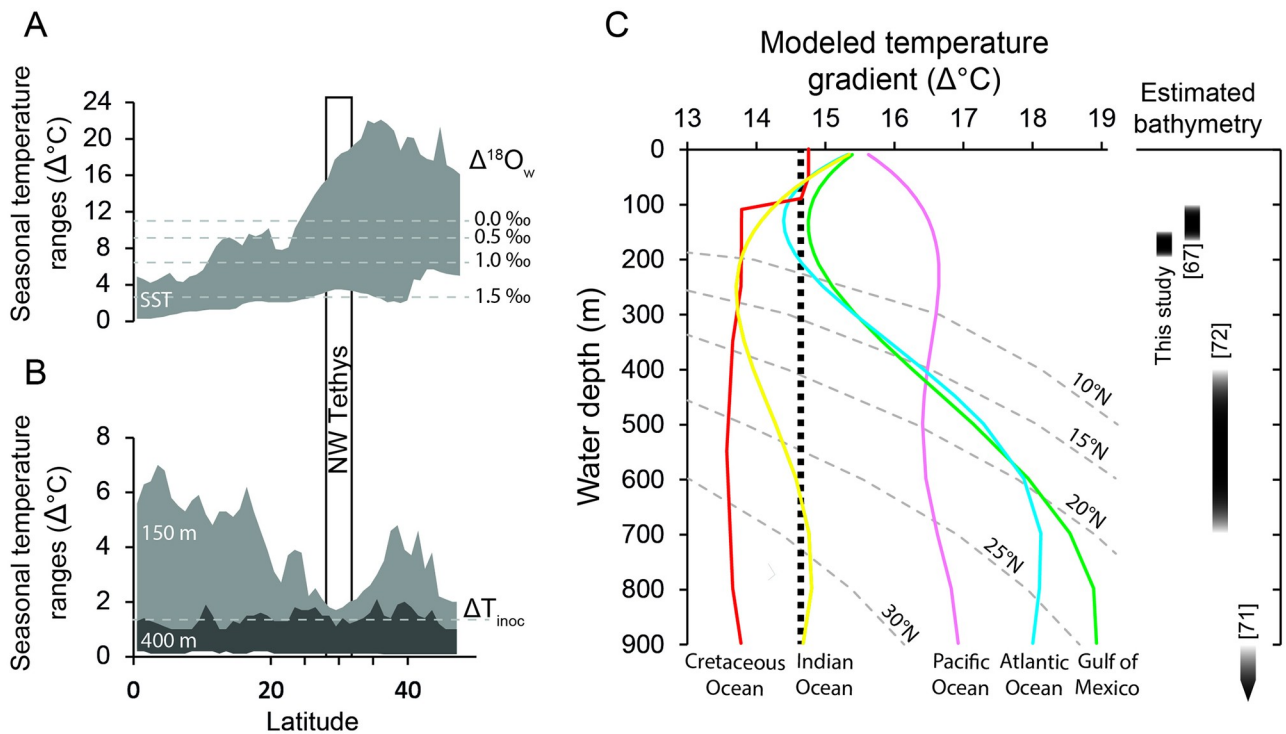
Fig 6. Comparison between inferred late Turonian/Early Coniacian water temperatures and observational data from modern tropical oceans.
(A) Annual water temperature amplitudes (ΔT) of the studied shallow water environment of the Tethys (dashed lines) reconstructed from the sclerochronologically sampled $\delta^{18}O$ values of the rudist shells (Fig 4A) are compared to the latitudinal changes of the seasonal near-surface (2.5–7.0 m) temperatures observed in modern oceans (gray shadow) [112]. When seasonal changes in $\delta^{18}O_w$ ($\Delta^{18}O_w$) are taken into account, the reconstructed ΔT ranges become narrower (see text for detailed explanation). (B) Similar to (A), the estimated seasonal ΔT amplitude for the hemipelagic environment was compared to observed ΔT ranges in modern oceans at 150 m (light gray) and 400 m (dark gray) water depth [112]. (C) Results of our model on the effect of bathymetrical $\delta^{18}O_w$ changes on the reconstruction of the vertical temperature gradient (see method for detailed explanation). Vertical ΔT gradients were calculated from the rudist and inoceramid data assuming the vertical $\delta^{18}O_w$ changes modeled for the Late Cretaceous oceans [82] as well as observed in the modern Indian (yellow), Pacific (pink), and Atlantic Oceans (blue) and the Gulf of Mexico (green) [83]. The gray dotted line depicts zonally averaged vertical ΔT gradients. Bathymetries (black bars) of the Trento Plateau inferred in the present and previous studies [67,71,72] are depicted to the right.

https://doi.org/10.1371/journal.pone.0238040.g006

that short-term variations of the water oxygen isotope signature had only a minor effect on $\delta^{18}O$-based temperature estimates.

In the context of the present study, we focused on the assessment of vertical temperature changes in the water column, and less on absolute reconstructions. However, the uncertainties in the temperature reconstructions highlighted above outline the importance to implement climate research with other proxy data.

Vertical temperature gradient and paleoclimate implications

The reconstructed seasonal $\delta^{18}O$ amplitudes suggest that rudists and inoceramids were exposed to waters with very different physical properties, e.g., different $\delta^{18}O_w$ signatures, temperatures, or a combination of both factors. As mentioned above, vertical changes in the $\delta^{18}O$ signal of the water could have played a role during the incorporation of oxygen isotopes. However, this effect was likely not dominant. In fact, to fully justify the 2.00 ‰ difference between the two shell $\delta^{18}O$ datasets (Fig 5), it is necessary to assume implausible $\delta^{18}O_w$ water signals for the two environments. According to Eq 1, the most positive and the most negative $\delta^{18}O$ values of the inoceramids and the rudists, respectively, would yield the same paleowater temperature if the surface $\delta^{18}O$ water equaled -3.00 ‰ (or, otherwise, a benthic $\delta^{18}O_w$ = 1.00 ‰).

According to the Late Cretaceous freshwater mixing line developed the western Interior Seaway waters [100], such a scenario implies an extraordinary input of freshwater/precipitation to the shallow environment. Accordingly, surface salinity should have been as low as 26 PSU, whereas, normal marine salinity conditions (34 PSU) would have existed at the bottom of the sea. Surface hypohyaline conditions, however, contrast with the highly diverse fully marine Gosau fauna at the studied locality [63,64]. Furthermore, such strong vertical gradient in salinity may have resulted in a density-driven stratification of the water column and reduced levels of oxygen in the benthic environment, as in the case of Western Interior Seaway in North America [100]. Stagnation and benthic hypoxia, however, are not consistent with the diverse macrofossil community of the 'lastame' lithofacies [66–72] and the presence of authigenic hematite, which indicate well-oxygenated conditions at the seafloor [18]. Therefore, it is reasonable to assume that the observed δ^{18}O difference between the studied rudists and inoceramids resulted from a combined effect of changing water temperature and δ^{18}O$_w$ signature.

Assuming modern-like vertical δ^{18}O$_w$ changes for the upper 900 m of the studied region, the proposed model yielded temperature gradients ranging between ca. 14 and 19 ˚C. Among the modeled scenarios, the most conservative ΔT estimates (13–14 ˚C; Late Cretaceous and Indian Ocean settings) were very close to the ΔT value (14–15 ˚C) computed with a homogeneous δ^{18}O$_w$ value. Therefore, we interpret the vertical effect of changing δ^{18}O$_w$ on the measured δ^{18}O$_{shell}$ amplitude as minor, and ascribe the isotopic differences between the rudist and inoceramid data to a heterogeneous thermal structure of the water body (Fig 5). The precise estimation of the vertical ΔT gradient, however, also depends on the assumed water depth for the Trento Plateau. The oxygen-rich water conditions postulated for the 'lastame' lithofacies [67] suggest that the studied environment was located above the oxygen minimum zone [72], which in tropical oceans can be generally positioned between 150 and 500 m water depth [113]. This range fits well with the shallower paleodepths assumed for the Trento Plateau in previous studies [67,72] and make a bathyal depth postulated by others unrealistic [71]. The presence of a diverse ratiolitid rudist fauna in the Scaglia Rossa deposits of Sant´Anna d´Alfaedo, however, provide a strong line of evidence that the studied nodular 'lastame' lithofacies was placed in the upper part (~150 m or slightly below) of this bathymetric range [72]. At a water depth between 150 and 200 m, the model suggested ΔT gradients between 13–14 (Late Cretaceous and Indian Ocean), 14–15 ˚C (Atlantic Ocean and Gulf of Mexico) and 16–17 ˚C (Pacific Ocean), which compare well to the vertical ΔT values observed in the modern tropical latitudes 10˚N (Fig 6C). Previous studies have postulated a poleward shift of ca. 5˚–10˚ for the tropic/sub-tropic belts during the Late Cretaceous [114]. The annual ΔT amplitudes inferred for the shallow water setting (ca. 30 ˚N) compare well with those observed in modern tropical waters (20˚-25 ˚N) and seem to fit in this frame. However, even in the context of the Late Cretaceous greenhouse world, it seems very unlikely that the near-equatorial scenario could have extended up to studied latitudes. Therefore, to explain the δ^{18}O difference between the rudists and inoceramid shells, we hypothesize the existence a heterogeneous structure of the water column at the northwestern Tethyan margin with a bottom source of cold hydrological masses. To enable an easy comparison with the literature data, in the following, temperature estimates will be reported assuming a seasonally constant δ^{18}O$_w$ value of -1.0 ‰.

The temperature estimates obtained from rudist shells (24–35 ˚C) are in the range of those reconstructed from fish tooth apatite of the region [21] (Fig 5). This suggests that surface conditions and atmospheric variability affected both the shallow water biotope and the upper layer of the Tethys Ocean (Fig 5). Such warm surface Tethyan-like conditions also likely pervaded the shallow water and shelf environments at higher latitudes at least during part of the Turonian, as suggested by the δ^{18}O data of brachiopods [12], rudist [84] and inoceramid shells [55] from Central European Basins. Short intervals of warm water conditions in the European mid-

latitudes are also supported by the northward extension of the biogeographic province of Tethyan ammonites [13]. On the contrary, the benthic water temperatures of the Trento Plateau are close to the conditions reconstructed for the shelf environments of Central Europe during the Hitch Wood Event (Fig 5). The Hitch Wood Event repents a short time interval of the Late Turonian during which boreal water masses spread into Central European basins and caused a continental-wide cooling of shelf sea waters [13,115]. Furthermore, an influence of water masses with boreal affinity on the Trento Plateau during the late Turonian–early Coniacian is compatible with the more or less coeval begin of deep water production in the North Atlantic [9,10], the inflow of oxygen-rich waters in the western sub-basins of the Tethys [115,116] and the increased uptake of unradiogenic neodymium isotopes in apatite of fish teeth of the Tethys [14].

The described thermal decoupling between bottom and shallow water habitats contrasts with the existence of an active upwelling system at the northwestern margin of the Tethys postulated by previous authors [14]. Although the published neodymium isotope data suggest some degree of vertical exchange in water column, our seasonally resolved temperature estimates clearly indicate that bottom waters did not reach the shallow water environment of the Helvetic Shelf. Furthermore, existing studies on shallow water filter-feeding bivalves show that exposure to upwelling events usually results in a linear relationship between $\delta^{13}C$ and $\delta^{18}O$ values of the shells [117–119]. Such a relationship, however, was not detected in the stable isotope values of the *V. inaequicostatus* (Figs 3A and 4A), for which a heterotrophic lifestyle can be assumed. The lack of a correlation between shell $\delta^{13}C$ and $\delta^{18}O$ values is typical for filter-feeding bivalves from shallow water habitats, where nutrient supply, primary production and water temperatures are controlled by surface seasonality [102]. The shell growth rates of the photosymbiotic *H. resectus* provide a further line of evidence for the shallow water environment being mainly controlled by surface dynamics. The metabolic response to heat stress among bivalves is heterogeneous. However, taxa able to grow their shells over water temperature changes of >12 ˚C are not uncommon (97,102). Following tank experiments short-term temperature rises by up to 6 ˚C can induce death of the symbiotic zooxanthellae and bleaching [120,121], without presenting a major metabolic stress for the bivalve host [120]. Furthermore, as discussed above, the annual ΔT amplitude of the Tethyan shallow water might have been lower than 11 ˚C, considering the effect of the seasonally changing $\delta^{18}O_w$ on the $\delta^{18}O_{shell}$ records of the rudists. Hence, it is likely that fluctuations in water temperatures did not represent a major obstacle for *H. resectus* to biomineralize. On the contrary, nutrient availability and irradiance are the two major limiting factors for shell growth in algae-bearing bivalves [45]. Since accretion rates in *H. resectus* decreased during summer (i.e., maximum seasonal irradiance), it is plausible that growth was mainly controlled by nutrient limitation. In this context, increased summer insolation might have boosted environmental photosynthetic activity leading to nutrient depletion of the upper photic zone in a comparable manner as observed in modern sub-tropical zones [122].

The positive correlation between $\delta^{13}C$ and $\delta^{18}O$ values of the inoceramids suggests that the process governing temperature fluctuations also affected food availability and/or the stable isotopic signature of the DIC on the Trento Plateau. The concomitant increase in food availability and temperature on the seafloor resulting from snowing of organic matter and advection of water masses from the surface has been invoked to explain the observed stable isotope pattern in previous Late Cretaceous studies [43,53]. However, as observed on modern basinal highs [123], seasonal changes in horizontal transport of particulate organic matter might have also played a role in the trophic balance of the environment. Additionally, bottom currents from the North Atlantic possibly provided a steady supply of cold and nutrient-rich waters to the lower photic zone, where weakened insolation determined coincidental fluctuations in

seasonal primary production and water temperatures. If this interpretation holds true, the present sclerochronogical data possibly suggest, to some extent, a decoupling also in the food webs between the shallow and bottom environments at the northwestern margin of the Tethys.

Conclusions

The present study highlights the potential of bivalve sclerochronology for Late Cretaceous paleoclimate reconstructions. Whereas most of the existing sclerochronological studies have focused on shallow water bivalves, information on the seasonality in deeper settings during this time interval is still very limited. As shown here, seasonally resolved environmental data from different taxa, which inhabited different water depths, can provide quantitative information on the internal structure of an ancient water column. Such data are often only available from numerical climate simulations and are of fundamental importance for paleoceanographic studies.

Our findings indicate the existence of a steep vertical temperature gradient of ca. 15 ˚C from the bottom to the surface of the northwestern Tethys Ocean during the late Turonian-early Coniacian. Such gradient is steeper than observed at modern tropical latitudes (20˚N–25˚N) under normal marine conditions and suggest the existence of a structurally heterogenous water body at the northwestern Tethyan margin. Bottom cooling was likely caused by benthic currents with old and nutrient-rich waters of North Atlantic origin. At the same time, however, strong radiative forcing at the surface resulted in the warmest conditions recorded over the entire Late Cretaceous in the shallow water habitats of the region. The substantial differences in the vertical water temperatures and their seasonal amplitudes suggest the existence of a perennial thermocline. The precise position of the latter remains unknown, however, it was likely located below the migratory depth of the ichthyofauna used for δ^{18}O-based temperature reconstructions [21]. Moreover, the stable isotopic patterns of the studied bivalve shells also suggest that the supply of North Atlantic waters to the lower photic zone may have resulted in a certain degree of independence between the trophic systems of the two environments. Hence, it is unlikely that an active upwelling system persisted in the region at that time, as postulated by previous authors.

Supporting information

S1 Fig.
(JPG)

S1 Data.
(XLSX)

Acknowledgments

Author Contributions

Conceptualization: Eric Otto Walliser, Bernd R. Schöne.

Data curation: Eric Otto Walliser, Bernd R. Schöne.

Formal analysis: Eric Otto Walliser, Bernd R. Schöne.

Funding acquisition: Bernd R. Schöne.

Investigation: Eric Otto Walliser.

Methodology: Eric Otto Walliser, Bernd R. Schöne.

Validation: Eric Otto Walliser.

Writing – original draft: Eric Otto Walliser, Bernd R. Schöne.

References

1. Clarke LJ, Jenkyns HC. New oxygen isotope evidence for long-term Cretaceous climatic change in the Southern Hemisphere. Geology 1999; 27(8):699–702.

2. Forster A, Schouten S, Baas M, Sinninghe Damsté JS. Mid-Cretaceous (Albian-Santonian) sea surface temperature record of the tropical Atlantic Ocean. Geology 2007; 35(10):919–922. https://doi.org/10.1130/G23874A.1

3. Miller KG, Wright JD, Browning JV. Visions of ice sheets in a greenhouse world. Mar Geol. 2005; 217 (3–4):215–231. https://doi.org/10.1016/j.margeo.2005.02.007

4. Friedrich O, Norris RD, Erbacher J. Evolution of middle to late Cretaceous oceans—a 55 m.y. record of Earth's temperature and carbon cycle. Geology 2012: 40(2):107–110. https://doi.org/10.1130/G32701.1

5. Linnert C, Robinson SA, Lees JA, Bown PR, Pérez-Rodríguez I, Petrizzo MR, et al. Evidence for global cooling in the Late Cretaceous. Nat Comm. 2014; 5:4194. https://doi.org/10.1038/ncomms5194 PMID: 24937202

6. Foster GL, Royer DL, Lunt DJ. Future climate forcing potentially without precedent in the last 420 million years. Nat Comm. 2017; 8:14845. https://doi.org/10.1038/ncomms14845 PMID: 28375201

7. Voigt S, Jung C, Friedrich O, Frank M, Teschner C, Hoffmann J. Tectonically restricted deep-ocean circulation at the end of the Cretaceous greenhouse. Earth Plan Sci Lett. 2013; 369:169–177. https://doi.org/10.1016/j.epsl.2013.03.019

8. Brady EC, DeConto RM, Thompson SL. Deep water formation and poleward ocean heat transport in the warm climate extreme of the Cretaceous (80 Ma). Geophys Res Lett. 1998; 25(22):4205–4208. https://doi.org/10.1029/1998GL900072

9. Poulsen CJ, Seidov D, Barron EJ, Peterson WH. The impact of paleogeographic evolution on the surface oceanic circulation and the marine environment within the Mid-Cretaceous Tethys. Paleoceanograp. 1998; 13(5):546–559. https://doi.org/10.1029/98PA01789

10. Otto-Bliesner BL, Brady EC, Shilelds C. Late Cretaceous ocean: coupled simulations with the National Center for Atmospheric Research Climate System Model. J Geophys Res. 2002; 107(D2):4019. https://doi.org/10.1029/2001JD000821

11. Bornemann A, Norris RD, Friedrich O, Beckmann B, Schouten S, Damsté JSS, et al. Isotopic evidence for glaciation during the Cretaceous supergreenhouse. Science 2008; 319(5860):189–192. https://doi.org/10.1126/science.1148777 PMID: 18187651

12. Voigt S, Gale AS, Flögel S. Midlatitude shelf seas in the Cenomanian-Turonian greenhouse world: temperature evolution and North Atlantic circulation. Paleoceanography 2004; 19(4):PA4020. https://doi.org/10.1029/2004PA001015

13. Wiese F, Voigt S. Late Turonian (Cretaceous) climate cooling in Europe: faunal response and possible causes. Geobios 2002; 35(1):65–77. https://doi.org/10.1016/S0016-6995(02)00010-4

14. Pucéat E, Lécuyer C, Reisberg L. Neodymium isotope evolution of NW Tethyan upper ocean waters throughout the Cretaceous. Earth Planet Sci Lett. 2005; 236(3–4):705–720. https://doi.org/10.1016/j.epsl.2005.03.015

15. Channell JET, Freeman R, Heller F, Lowrie W. Timing of diagenetic hematite growth in red pelagic limestones from Gubbio (Italy). Earth Plan Sci Lett. 1982; 58(2),189–201. https://doi.org/10.1016/0012-821X(82)90193-5

16. Cai Y, Li X, Hu X, Chen X, Pan Y. Paleoclimatic approach to the origin of the coloring of Turonian pelagic limestones from the Vispi Quarry section (Cretaceous, central Italy). Cret Res. 2009; 30 (5):1205–1216. https://doi.org/10.1016/j.cretres.2009.06.002

17. Neuhuber S, Wagreich M. Geochemistry of Cretaceous Oceanic Red Beds—a synthesis. Sed Geol. 2011; 235(1–2):72–78. https://doi.org/10.1016/j.sedgeo.2010.10.008

18. Hu X, Jansa L, Sarti M. Mid-Cretaceous oceanic red beds in the Umbria-Marche Basin, central Italy: constraints on paleoceanography and paleoclimate. Palaeogeogr Palaeoclimatol Palaeoecol. 2005; 233(3–4):163–186. https://doi.org/10.1016/j.palaeo.2005.10.003

19. Wagreich M. Coniacian-Santonian Oceanic Red Beds and their link to Oceanic Anoxic Event 3. SEPM Special Publications 2009; 91:235–242.

20. Wang C, Hu X, Huang Y, Wagreich M, Scott R, Hay W. Cretaceous Oceanic Red Beds as possible consequence of Oceanic Anoxic Events. Sed Geol. 2011; 235(1):27–37. https://doi.org/10.1016/j.sedgeo.2010.06.025

21. Pucéat C, Sheppard SMF, Dromart G. Thermal evolution of Cretaceous Tethyan marine waters inferred from oxygen isotope composition of fish tooth enamels. Paleocenogr. 2003; 18(2):1029. https://doi.org/10.1029/2002PA000823

22. Steuber T, Rauch M, Masse J- P, Graaf J, Malkoc M. Low-latitude seasonality of Cretaceous temperatures in warm and cold episodes. Nature 2005; 437:1341–1344. https://doi.org/10.1038/nature04096 PMID: 16251961

23. Abboud-Abi Saab M, Romano JC, Bensoussan N, Fakhri M. Suivis temporels comparés de la structure thermique d'eaux côtières libanaises (Batroun) et françaises (Marseille) entre juin 1999 et octobre 2002. Compt Rend Geosci. 2004; 336:1379–1390. https://doi.org/10.1016/j.crte.2004.09.004

24. Mignot J, de Boyer Montégut C, Lazar A, Cravatte S. Control of salinity on the mixed layer depth in the world ocean: 2. Tropical areas. J Geophys Res Oc. 2007; 112(10):C10010. https://doi.org/10.1029/2006JC003954

25. Pietri A, Testor P, Echevin V, Chaigneau A, Mortier L, Eldin G, Grados C. Finescale vertical structure of the upwelling system off southern Peru as observed from glider data. J Phys Oceanogr. 2013; 43 (3):631–646. https://doi.org/10.1175/JPO-D-12-035.1

26. García-Reyes M, Largier JL. Seasonality of coastal upwelling off central and northern California: New insights, including temporal and spatial variability. J Geophys Res Oc. 2012; 117(C3):C03028. https://doi.org/10.1029/2011JC007629

27. Chenillat F, Rivière P, Capet X, Di Lorenzo E, Blanke B. North Pacific Gyre Oscillation modulates seasonal timing and ecosystem functioning in the California Current upwelling system. Geophys Res Lett. 2012; 39(1):L01606. https://doi.org/10.1029/2011GL049966

28. Gili E, Masse JP, Skelton PW. Rudists as gregarious sediment-dwellers, not reef-builders, on Cretaceous carbonate platforms. Palaeogeogr Palaeoclimatol Palaeoecol. 1995; 118(3–4):245–267. https://doi.org/10.1016/0031-0182(95)00006-X

29. Skelton PW. Rudist evolution and extinction—a North African perspective. In: Gili E., Negra H., Skelton P.W. (Eds.), North African Cretaceous carbonate platform systems, NATO Sci. Ser. IV: Earth Environ. Sci. 2003; 28:215–227. Kluver Academic Publisher, Dordrecht. https://doi.org/10.1007/978-94-010-0015-4_13

30. Steuber T. Stable isotope sclerochronology of rudist bivalves: growth rates and Late Cretaceous seasonality. Geology 1996; 24(4):315–318.

31. Steuber T, Yilmaz C, Löser H. Growth rates of early Campanian rudists in a siliciclastic-calcareous setting (Pontid MTS., North-Central Turkey). *Geobios* 1998; 31(1):385–401. https://doi.org/10.1016/S0016-6995(98)80088-0

32. Steuber T. Isotopic and chemical intra-shell variations in low-Mg calcite of rudist bivalves (Mollusca—Hippuritacea): disequilibrium fractionations and late Cretaceous seasonality. Int J Earth Sci. 1999; 88:551–570. https://doi.org/10.1007/s005310050284

33. de Winter NJ, Goderis S, Van Malderen SJ, Sinnesael M, Vansteenberge S, Snoeck C, Belza J, Vanhaecke F, Claeys P. Sub-daily scale chemical variability in a *Torreites sanchezi* rudist shell: Implications for rudist paleobiology and the Cretaceous day-night cycle. Paleoceanogr Paleoclimatol. 2020; 35(2): e2019PA003723. https://doi.org/10.1029/2019PA003723

34. Dhondt AV. Cretaceous inoceramid biogeography: a review. Palaeogeogr Palaeoclimatol Palaeoecol.1992; 92(3–4):217–232. https://doi.org/10.1016/0031-0182(92)90083-H

35. Tourtelot HA, Rye RO. Distribution of oxygen and carbon isotopes in fossils of Late Cretaceous age, Western Interior region of North America. Geol Soc Am Bull. 1969; 80(10):1903–1922. https://doi.org/10.1130/0016-7606(1969)80[1903:DOOACI]2.0.CO;2

36. Pirrie D, Marshall JD. Diagenesis of *Inoceramus* and Late Cretaceous paleoenvironmental geochemistry: a case study from James Ross Island, Antarctica. PALAIOS 1990; 5(4):336–345. https://doi.org/10.2307/3514889

37. Ludvigson GA, Witzke BJ, Gonzalez LA, Hammond RH, Plocher OW. Sedimentology and carbonate geochemistry of concretions from the Greenhorn marine cycle (Cenomanian-Turonian), eastern margin of the Western Interior Seaway. Geol Soc Am Special Paper 1994; 287:145–174. https://doi.org/10.1130/SPE287-p145

38. Elorza J, Garcia-Garmilla F. Petrological and geochemical evidence for diagenesis of inoceramid bivalve shells in the Plentzia Formation (Upper Cretaceous, Basque-Cantabrian Region, northern Spain). Cret Res. 1996; 17(4):479–503. https://doi.org/10.1006/cres.1996.0029

39. Fisher CG, Arthur MA. Water mass characteristics in the Cenomanian US Western Interior seaway as indicated by stable isotopes of calcareous organisms. Palaeogeogr Palaeoclimatol Palaeoecol. 2002; 188(3–4):189–213. https://doi.org/10.1016/S0031-0182(02)00552-7

40. He S, Kyser TK, Caldwell WGE. Paleoenvironment of the Western Interior Seaway inferred from $\delta^{18}O$ and $\delta^{13}C$ values of molluscs from the Cretaceous Bearpaw marine cyclothem. Palaeogeogr Palaeoclimatol Palaeoecol. 2005; 217(1–2):67–85. https://doi.org/10.1016/j.palaeo.2004.11.016

41. Henderson RA, Price GD. Paleoenvironment and paleoecology inferred from oxygen and carbon isotopes of subtropical mollusks from the Late Cretaceous (Cenomanian) of Bathurst Island, Australia. PALAIOS 2012; 27:617–626. https://doi.org/10.2110/Palo.2011.P11-120r

42. Zakharov YD, Smyshlyaeva OP, Popov AM, Velivetskaya TA, Afanasyeva TB, Tanabe K, Shigeta Y, Maeda H. Pole to equator temperature gradient for Coniacian time, Late Cretaceous: oxygen and carbon isotopic data on the Koryak upland and Hokkaido. J Earth Sci 2012; 23(1):19–32. https://doi.org/10.1007/s12583-012-0230-0

43. Walliser EO, Tanabe K, Hikida Y, Shirai K, Schöne BR. Sclerochronological study of the gigantic inoceramids *Sphenoceramus schmidti* and *S. sachalinensis* from Hokkaido, northern Japan. Lethaia 2019; 52(3):410–428. https://doi.org/10.1111/let.12321

44. Vermeij GJ. The evolution of molluscan photosymbioses: a critical appraisal. Biol Jof Linn Soc. 2013; 109(3):497–511. https://doi.org/10.1111/bij.12095

45. McConnaughey TA, Gillikin DP. Carbon isotopes in mollusk shell carbonates. Geo-Mar Lett. 2008; 28 (5):287–299. https://doi.org/10.1007/s00367-008-0116-4

46. Warter V, Erez J, Müller W. Environmental and physiological controls on daily trace element incorporation in *Tridacna crocea* from combined laboratory culturing and ultra-high resolution LA-ICP-MS analysis. Palaeogeogr Palaeoclimatol Palaeoecol. 2018; 496:32–47. https://doi.org/10.1016/j.palaeo.2017.12.038

47. Watanabe T, Oba T. Daily reconstruction of water temperature from oxygen isotopic ratios of a modern Tridacna shell using a freezing microtome sampling technique. J Geophys Res O. 1999; 104 (C9):20667–20674. https://doi.org/10.1029/1999JC900097

48. Watanabe T, Suzuki A, Kawahata H, Kan H, Ogawa S. A 60-year isotopic record from a mid-Holocene fossil giant clam (Tridacna gigas) in the Ryukyu Islands: physiological and paleoclimatic implications. Palaeogeogr. Palaeoclimatol. Palaeoecol. 2004; 212(3–4):343–354. https://doi.org/10.1016/j.palaeo.2004.07.001

49. Jones DS, Williams DF, Spero HJ. More light on photosymbiosis in fossil mollusks: the case of Mercenaria "tridacnoides". Palaeogeogr. Palaeoclimatol. Palaeoecol. 1988; 64(3–4):141–52. https://doi.org/10.1016/0031-0182(88)90003-X

50. Seilacher A. Aberrations in bivalve evolution related to photo-and chemosymbiosis. Hist. Biol. 1990; 3 (4):289–311. https://doi.org/10.1080/08912969009386528

51. Cowen R. Algal symbiosis and its recognition in the fossil record. In Biotic interactions in Recent and Fossil Benthic Communities. 1983; pp. 431–478. Springer, Boston, MA.

52. MacLeod KG, Hoppe KA. Evidence that inoceramid bivalves were benthic and harbored chemosynthetic symbionts. Geology 1992; 20(2):117–120.

53. Jiménez Berrocoso Á, MacLeod KG, Calvert SE, Elorza J. Bottom water anoxia, inoceramid colonization, and benthopelagic coupling during black shale deposition on Demerara Rise (Late Cretaceous western tropical North Atlantic). Paleoceanogr. 2008; 23(3):PA3212. https://doi.org/10.1029/2007PA001545

54. Walliser EO, Mertz-Kraus R, Schöne BR. The giant inoceramid *Platyceramus platinus* as a high-resolution paleoclimate archive for the Late Cretaceous of the Western Interior Seaway. Cret Res. 2018; 86:73–90. https://doi.org/10.1016/j.cretres.2018.01.010

55. Walliser EO, Vodrážka R, Höche N, Voigt S, Schöne BR. Late Turonian climate variability in the Bohemian Cretaceous Basin–A sclerochronological study of the *Inoceramus hercules* shells from the Úpohlavy working quarry (Czech Republic). Palaeogeogr Palaeoclimatol Palaeoecol. in review.

56. Landman NH, Cochran JK, Larson NL, Brezina J, Garb MP, Harries PJ. Methane seeps as ammonite habitats in the US Western Interior Seaway revealed by isotopic analyses of well-preserved shell material. Geology. 2012; 40(6):507–10. https://doi.org/10.1130/G32782.1

57. Kauffman EG, Harries PJ, Meyer C, Villamil T, Arango C, Jaecks G. Paleoecology of giant Inoceramidae (*Platyceramus*) on a Santonian (Cretaceous) seafloor in Colorado. J Paleontol. 2007; 81(1):64–81. https://doi.org/10.1666/0022-3360(2007)81[64:POGIPO]2.0.CO;2

58. Rio M, Roux M, Renard M, Schein E. Chemical and isotopic features of present day bivalve shells from hydrothermal vents or cold seeps. Palaios 1992; 7(4):351–60. https://doi.org/10.2307/3514821

59. Lietard C, Pierre C. Isotopic signatures ($\delta^{18}O$ and $\delta^{13}C$) of bivalve shells from cold seeps and hydrothermal vents. Geobios 2009; 42(2):209–19. https://doi.org/10.1016/j.geobios.2008.12.001

60. Lartaud F, De Rafélis M, Oliver G, Krylova E, Dyment J, Ildefonse B, Thibaud R, Gente P, Hoisé E, Meistertzheim AL, Fouquet Y. Fossil clams from a serpentinite-hosted sedimented vent field near the active smoker complex Rainbow, MAR, 36 13′ N: Insight into the biogeography of vent fauna. Geochem. Geophys. Geosyst. 2010; 11(8):Q0AE01. https://doi.org/10.1029/2010GC003079

61. Nedoncelle K, Le Bris N, de Rafélis M, Labourdette N, Lartaud F. Non-equilibrium fractionation of stable carbon isotopes in chemosynthetic mussels. Chem. Geol. 2014; 387:35–46. https://doi.org/10.1016/j.chemgeo.2014.08.002

62. Smith AG, Smith DG, Funnell BM. Atlas of Mesozoic and Cenozoic coastlines. Cambridge University Press; 2004, pp. 99.

63. Sanders D, Baron-Szabo RC. Coral-Rudist bioconstructions in the Upper Cretaceous Haidach section (Gosau Group; Northern Calcareous Alps, Austria). Facies 1997; 36(1):69–90. https://doi.org/10.1007/BF02536878

64. Sanders D, Pons JM. Rudist formations in mixed siliciclastic-carbonate depositional environments, Upper Cretaceous, Austria: stratigraphy, sedimentology, and models of development. Palaeogeogr Palaeoclimatol Palaeoecol. 1999; 148(4):249–284. https://doi.org/10.1016/S0031-0182(98)00186-2

65. Rauch M. Geochemie von Rudistenschalen-Beiträge zur Meerwasserchemie (Sr/Ca, Mg/Ca, δ13C) und Paläoklima der Kreide. Doctoral dissertation, Ruhr-University of Bochum. 2005. https://hss-opus.ub.ruhr-uni-bochum.de/opus4/frontdoor/deliver/index/docId/4079/file/diss.pdf.

66. Massari F, Savazzi E. Driftwood transportation and exotic pebbles in the Upper Cretaceous Scaglia Rossa veneta (M. Loffa, Southern Alps) suggested by Teredinid tubes. N Jah Geol Pal Abh. 1981; 5:311–320.

67. Trevisani E., Cestari R. Upper Cretaceous bivalves from basinal highs (Venetian Prealps, northern Italy). In: Scott R.W. (Ed.), Cretaceous Rudists and Carbonate Platforms: Environmental Feedback, SEPM Special Publication 2007; 87:71–80. https://doi.org/10.2110/pec.07.87.0071.

68. Zorzin R. Vertebrati fossili marini e terrestri del Veronese. 1st ed. Verona: Cierre Edizioni; 2017.

69. Amalfitano J, Dalla Vecchia FM, Giusberti L, Fornaciari E, Luciani V, Roghi G. Direct evidence of trophic interaction between a large lamniform shark, *Cretodus* sp., and a marine turtle from the Cretaceous of northeastern Italy. Palaeogeogr Palaeoclimatol Palaeoecol. 2017; 469:104–121. https://doi.org/10.1016/j.palaeo.2016.12.044

70. Amalfitano J, Giusberti L, Dalla Vecchia FM, Kriwet J. First skeletal remains of the giant sawfish *Onchosaurus* (Neoselachii, Sclerorhynchiformes) from the Upper Cretaceous of northeastern Italy. Cret Res. 2017; 69:124–135. https://doi.org/10.1016/j.cretres.2016.09.005

71. Venturini S. Ammoniti e rudiste nel 'lastame' della diga foranea di Grado (Gorizia): una curiosità paleontologica ed un problema paleoambientale. Nat Nasc. 2012; 44:10–20.

72. Bosellini A, Loriga C, Busetto C. I bacini cretacei del Trentino. Riv. Ital. Paleont. 1978; 84: 897–946.

73. Summesberger H, Kennedy WJ. Turonian ammonites from the Gosau Group (Upper Cretaceous; Northern Calcareous Alps; Austria) with a revision of *Barroisiceras haberfellneri* (HAUER, 1866). Beitr. Paläontol. 1996; 21:105–177.

74. Steuber T. Strontium isotope stratigraphy of Turonian-Campanian Gosau-type rudist formations in the Northern Calcareous and Central Alps (Austria and Germany). Cret Res. 2001; 22(4):429–441. https://doi.org/10.1006/cres.2001.0268

75. Ogg JG, Ogg GM, Gradstein FM. A concise geologic time scale. Elsevier 2016, pp.234.

76. Machel HG, Mason RA, Mariano AN, Mucci A. Causes and emission of luminescence in calcite and dolomite. In: Barker C.E. & Kopp O.C. (Eds): Luminescence Microscopy and Spectroscopy: Qualitative and Quantitative Applications. SEPM Short Courses Notes 1991; 25: 9–25. https://doi.org/10.2110/scn.91.25.0009

77. Major RP. Cathodoluminescence in post-Miocene carbonates. In: Barker C.E. & Kopp O.C. (Eds): Luminescence Microscopy and Spectroscopy: Qualitative and Quantitative Applications. SEPM Short Courses Notes 1991; 25:149–155. https://doi.org/10.2110/scn.91.25.0149

78. Frija G, Parente M, Di Lucia M, Mutti M. Carbon and strontium isotope stratigraphy of the Upper Cretaceous (Cenomanian-Campanian) shallow-water carbonates of southern Italy: Chronostratigraphic calibration of larger foraminifera biostratigraphy. Cret Res. 2015; 53:110–139. https://doi.org/10.1016/j.cretres.2014.11.002

79. Mook WG. Paleotemperatures and chlorinities from stable carbon and oxygen isotopes in shell carbonate. Palaeogeogr Palaeoclimatol Palaeoecol. 1971; 9(4):245–263. https://doi.org/10.1016/0031-0182(71)90002-2

80. Anderson TK, Arthur MA. Stable isotopes of oxygen and carbon and their application to sedimentologic and paleoenvironmental problems. SEPM Short Course 1983; 10:1–151. https://doi.org/10.2110/scn.83.01.0000

81. Shackleton NJ, Kennett JP. Paleotemperature history of the Cenozoic and the initiation of Antarctic glaciation: oxygen and carbon isotope analyses in DSDP Sites 277, 279 and 281. In Rep Deep Sea Drill Pr. 1975; 29:743–755. https://doi.org/10.2973/dsdp.proc.29.117.1975

82. Zhou J, Poulsen CJ, Pollard D, White TS. Simulation of modern and middle Cretaceous marine $\delta^{18}O$ with an ocean-atmosphere general circulation model. Paleoceanograp. 2008; 23(3):PA3223. https://doi.org/10.1029/2008PA001596

83. Schmidt GA, Bigg GR, Rohling EJ. "Global Seawater Oxygen-18 Database—v1.22". 1999. https://data.giss.nasa.gov/o18data/

84. El-Shazly S, Košťák M, Abdel-Gawad G, Kloučková B, Saber SG, Felieh Salama Y, Mazuch M, Žák K. Carbon and oxygen stable isotopes of selected Cenomanian and 663 Turonian rudists from Egypt and Czech Republic, and a note on changes in rudist 664 diversity. Bull Geosci. 2011; 86(2):209–226. https://doi.org/10.3140/bull.geosci.1151

85. Košťák M, Wiese F. Extremely rare Turonian belemnites from the Bohemian Cretaceous Basin and their palaeogeographical importance. Act Palaeontol Pol. 2011; 56:433–437.

86. Immenhauser A, Nägler TF, Steuber T, Hippler D. A critical assessment of mollusk $^{18}O/^{16}O$, Mg/Ca, and $^{44}Ca/^{40}Ca$ ratios as proxies for Cretaceous seawater temperature seasonality. Palaeogeogr Palaeoclimatol Palaeoecol. 2005; 215(3–4):221–237. https://doi.org/10.1016/j.palaeo.2004.09.005

87. Walliser EO, Fröhlich L, Vonhof H, Schöne BR. An evaluation of inoceramid single-prism sclerochronology. Palaeogeogr Palaeoclimatol Palaeoecol. 2020; 547:109690. https://doi.org/10.1016/j.palaeo.2020.109690

88. Ivany LC. Reconstructing paleoseasonality from accretionary skeletal carbonates—challenges and opportunities. Paleontol Soc Papers 2012; 18:133–166. https://doi.org/10.1017/S108933260000259X

89. Flügel E. Microfacies of carbonate rocks: analysis, interpretation and application. Berlin: Springer; 2004.

90. Carpenter SJ, Erickson JM, Lohmann KC, Owen MR. Diagenesis of fossiliferous concretions from the Upper Cretaceous Fox Hills Formation, North Dakota. J. Sediment. Res. 1988; 58(4):706–23. https://doi.org/10.1306/212F8E27-2B24-11D7-8648000102C1865D

91. Jenkyns HC, Gale AS, Corfield RM. Carbon-and oxygen-isotope stratigraphy of the English Chalk and Italian Scaglia and its palaeoclimatic significance. Geol Mag. 1994; 131(1):1–34. https://doi.org/10.1017/S0016756800010451

92. Fantle MS, Maher KM, Depaolo DJ. Isotopic approaches for quantifying the rates of marine burial diagenesis. Rev Geophys. 2010; 48(3):1–38. https://doi.org/10.1029/2009RG000306

93. Moriya K, Nishi H, Kawahata H, Tanabe K, Takayanagi Y. Demersal habitat of Late Cretaceous ammonoids: evidence from oxygen isotopes for the Campanian (Late Cretaceous) northwestern Pacific thermal structure. Geology 2003; 31(2):167–170.

94. Berry WBN, Barker RM. Fossil bivalve shells indicate longer month and year in Cretaceous than present. Nature 1968; 217:938–939. https://doi.org/10.1038/217938b0

95. Goodwin DH, Schöne BR, Dettman DL. Resolution and fidelity of oxygen isotopes as paleotemperature proxies in bivalve mollusk shells: models and observations. PALAIOS 2003; 18(2):110–125.

96. Steuber T. Stable isotope sclerochronology of *Vaccinites cornuvaccinum* (Hippuritidae) from Beotia (Greece). Rev Mex Cienc Geol. 1995; 12(2):307–314.

97. Peharda M, Thébault J, Markulin K, Schöne BR, Janeković I, Chauvaud L. Contrasting shell growth strategies in two Mediterranean bivalves revealed by oxygen-isotope ratio geochemistry: The case of *Pecten jacobaeus* and *Glycymeris pilosa*. Chem Geol. 2019; 526:23–35. https://doi.org/10.1016/j.chemgeo.2017.09.029

98. Auclair AC, Joachimski MM, Lécuyer C. Deciphering kinetic, metabolic and environmental controls on stable isotope fractionations between seawater and the shell of Terebratalia transversa (Brachiopoda). Chem Geol. 2003; 202(1–2):59–78. https://doi.org/10.1016/S0009-2541(03)00233-X

99. Yamamoto K, Asami R, Iryu Y. Within-shell variations in carbon and oxygen isotope compositions of two modern brachiopods from a subtropical shelf environment off Amami-o-shima, southwestern Japan. Geochem Geophy Geosyst. 2010; 11(10):Q10009. https://doi.org/10.1029/2010GC003190

100. Petersen SV, Tabor CR, Lohmann KC, Poulsen CJ, Meyer KW, Carpenter SJ, Erickson JM, Matsunaga KKS, Smith SY, Sheldon ND. Temperature and salinity of the Late Cretaceous Western Interior Seaway. Geology 2016; 44(11):903–906. https://doi.org/10.1130/G38311.1

101. Zakharov YD, Smyshlyaeva OP, Tanabe K, Shigeta Y, Maeda H, Ignatiev AV, Velivetskaya TA, Afanasyeva TB, Popov AM, Golozubov VV, Kolyada AA, Cherbadzhia AK, Moriya K. Seasonal temperature fluctuations in the high northern latitudes during the Cretaceous Period: isotopic evidence from Albian and Coniacian shallow-water invertebrates of the Talovka River Basin, Koryak Upland, Russian Far East. Cret Res. 2005; 26(1):113–32. https://doi.org/10.1016/j.cretres.2004.11.005

102. Peharda M, Walliser EO, Markulin K, Purroy A, Uvanović H, Janeković I, Župan I, Vilibić I, Schöne BR. Glycymeris pilosa (Bivalvia)—A high-potential geochemical archive of the environmental variability in the Adriatic Sea. Mar Envir Res. 2019; 150:104759. https://doi.org/10.1016/j.marenvres.2019.104759 PMID: 31344588

103. Schöne BR. The curse of physiology—challenges and opportunities in the interpretation of geochemical data from mollusk shells. Geo-Mar Lett. 2008; 28(5–6):269–285. https://doi.org/10.1007/s00367-008-0114-6

104. Lorrain A, Paulet Y-M, Chauvaud L, Dunbar R, Mucciarone D, Fontugne M. δ^{13}C variation in scallop shells: increasing metabolic carbon contribution with body size? Geochim Cosmochim Act. 2004; 68 (17):3509–3519. https://doi.org/10.1016/j.gca.2004.01.025

105. Poulain C, Lorrain A, Mas R, Gillikin DP, Dehairs F, Robert R, Paulet Y-M. Experimental shift of diet and DIC stable carbon isotopes: influence on shell δ^{13}C values in the Manila clam *Ruditapes philippinarum*. Chem Geol. 2010; 272(1–4):75–82. https://doi.org/10.1016/j.chemgeo.2010.02.006

106. Ivany LC, Brey T, Huber M, Buick DP, Schöne BR. El Niño in the Eocene greenhouse recorded by fossil bivalves and wood from Antarctica. Geophys Res Lett. 2011; 38(16):L16709. https://doi.org/10.1029/2011GL048635

107. Goodwin DH, Gillikin DP, Roopnarine PD. Preliminary evaluation of potential stable isotope and trace element productivity proxies in the oyster Crassostrea gigas. Palaeogeogr Palaeoclimatol Palaeoecol. 2013; 373:88–97. https://doi.org/10.1016/j.palaeo.2012.03.034

108. Walliser EO, Lohmann G, Niezgodzki I, Schöne BR. Inter-annual climate variability in Europe during the Oligocene icehouse. Palaeogeogr Palaeoclimatol Palaeoecol. 2017; 475:140–153. https://doi.org/10.1016/j.palaeo.2017.03.020

109. Goericke R, Fry B. Variations of marine plankton δ^{13}C with latitude, temperature, and dissolved CO_2 in the world ocean. Glob Biogeochem Cycl. 1994; 8(1):85–90. https://doi.org/10.1029/93GB03272

110. Benthien A, Zondervan I, Engel A, Hefter J, Terbrüggen A, Riebesell U. Carbon isotopic fractionation during a mesocosm bloom experiment dominated by *Emiliania huxleyi*: effects of CO_2 concentration and primary production. Geochim Cosmochim Act. 2007; 71(6):1528–1541. https://doi.org/10.1016/j.gca.2006.12.015

111. O'Brien CL, Robinson SA, Pancost RD, Damsté JS, Schouten S, Lunt DJ, Alsenz H, Bornemann A, Bottini C, Brassell SC, Farnsworth A. Cretaceous sea-surface temperature evolution: Constraints from TEX$_{86}$ and planktonic foraminiferal oxygen isotopes. Earth-Sci Rev. 2017; 172:224–47. https://doi.org/10.1016/j.earscirev.2017.07.012

112. Locarnini RA, Mishonov AV, Baranova OK, Boyer TP, Zweng MM, Garcia HE, Reagan JR, Seidov D, Weathers K, Paver CR, Smolyar I. World Ocean Atlas 2018, Volume 1: Temperature. In Mishonov A (ed.), 2018 NOAA Atlas NESDIS 81 20018; 52 pp.

113. Karstensen J, Stramma L, Visbeck M. Oxygen minimum zones in the eastern tropical Atlantic and Pacific oceans. Prog Oceanograph. 2008; 77(4):331–50. https://doi.org/10.1016/j.pocean.2007.05.009

114. Wagner T, Hofmann P, Flögel S. Marine black shale deposition and Hadley Cell dynamics: A conceptual framework for the Cretaceous Atlantic Ocean. Mar Petrol Geol. 2013; 43:222–38. https://doi.org/10.1016/j.marpetgeo.2013.02.005

115. Jarvis I, Trabucho-Alexandre J, Gröcke DR, Uličný D, Laurin J. Intercontinental correlation of organic carbon and carbonate stable isotope records: evidence of climate and sea-level change during the Turonian (Cretaceous). Dep Rec. 2015; 1(2):53–90. https://doi.org/10.1002/dep2.6

116. Hu XM, Cheng WB, Ji JF. Origin of Cretaceous oceanic red beds from the Vispi Quarry section, central Italy: visible reflectance and inorganic geochemistry. SEPM Special Publication 2009; 91:183–197.

117.   Killingley JS, Berger WH. Stable isotopes in a mollusk shell: detection of upwelling events. Science 1979; 205(4402):186–188. https://doi.org/10.1126/science.205.4402.186 PMID: 17750319

118.   Carré M, Bentaleb I, Blamart D, Ogle N, Cardenas F, Zevallos S, Kalin RM, Ortlieb L, Fontugne M. Stable isotopes and sclerochronology of the bivalve Mesodesma donacium: potential application to Peruvian paleoceanographic reconstructions. Palaeogeogr Palaeoclimatol Palaeoecol. 2005; 228(1–2):4–25. https://doi.org/10.1016/j.palaeo.2005.03.045

119.   Sadler J, Carré M, Azzoug M, Schauer AJ, Ledesma J, Cardenas F, Chase BM, Bentaleb I, Muller SD, Mandeng M, Rohling EJ. Reconstructing past upwelling intensity and the seasonal dynamics of primary productivity along the Peruvian coastline from mollusk shell stable isotopes. Geochem Geophys Geosyst. 2012; 13(1):Q01015. https://doi.org/10.1029/2011GC003595

120.   Dubousquet V, Gros E, Berteaux-Lecellier V, Viguier B, Raharivelomanana P, Bertrand C, Lecellier GJ. Changes in fatty acid composition in the giant clam *Tridacna maxima* in response to thermal stress. Biol Op. 2016; 5(10):1400–7. https://doi.org/10.1242/bio.017921 PMID: 27543058

121.   Zhou Z, Liu Z, Wang L, Luo J, Li H. Oxidative stress, apoptosis activation and symbiosis disruption in giant clam *Tridacna crocea* under high temperature. Fish Shellf. Immunol. 2019; 84:451–7. https://doi.org/10.1016/j.fsi.2018.10.033 PMID: 30315860

122.   Teira E, Mourino B, Maranon E, Perez V, Pazo MJ, Serret P. Variability of chlorophyll and primary production in the Eastern North Atlantic subtropical gyre: potential factors affecting phytoplankton activity. Deep Sea Res Oceanograph Res Pap. 2005; 52(4):569–588. https://doi.org/10.1016/j.dsr.2004.11.007

123.   Nodder SD, Pilditch CA, Probert PK, Hall JA. Variability in benthic biomass and activity beneath the Subtropical Front, Chatham Rise, SW Pacific Ocean. Deep Sea Res Part I: Oceanograph Res Pap. 2003; 50(8):959–85. https://doi.org/10.1016/S0967-0637(03)00094-3